NILU OR: 26/96

NILU : OR 26/96
REFERENCE : O-93003/O-96044
DATE : JULY 1996
ISBN : 82-425-0768-6

Radiative impacts of ozone and other radiatively active components

Frode Stordal, Terje A. Larsen, Gunnar Myhre og Lars Zetterberg

NILU : OR 26/96
REFERENCE : O-93003/O-96044
DATE : MARCH 1996
ISBN : 82-425-0768-6

Radiative impacts of ozone and other radiatively active components

Frode Stordal[1], Terje A. Larsen[1], Gunnar Myhre[2] og Lars Zetterberg[3]

1) Norwegian Institute for Air Research,
P.O. Box 100, N-2007 Kjeller, Norway

2) University of Oslo, Institute of Geophysics,
P.O. Box 1022 Blindern, N-0315 Oslo, Norway

3) Swedish Environmental Research Institute,
P.O. Box 47086, S-402 58 Göteborg, Sweden

Contents

Page

Summary

The transfer of radiation in the atmosphere has been simulated by a broad band model of long wave radiation and a spherical model of short wave radiation. The models have been used to study the impact of ozone on the radiative balance of the atmosphere. These calculations were made in order to assess both the role of ozone in the present atmosphere as well as the effects of observed changes in ozone over the last decades, both in the stratosphere and the troposphere.

Calculations based on ozone soundings at 3 Nordic sites show a marked seasonal cycle in the net radiative irradiance through the tropopause, denoted as the radiative forcing, both for long wave and short wave radiation. For the long wave radiation the seasonal variation is driven mainly by the variation in the temperature and the concentration of ozone, and is not much influenced by the seasonal cycle of the water vapour content. There is a distinct seasonal variation also in the short wave radiative irradiance through the tropopause. This has been calculated to be mainly due to the variation in the solar zenith angle, but also to some extent in the ozone concentration. The seasonal variation in the surface albedo is shown to be of less importance.

Extrapolations to the global atmosphere have also been made. Global climatological data for ozone and other climate gases as well as temperature, and cloud distribution, have been used as a basis for global radiatiave transfer calculations. Calculations performed in the infrared spectral region show that there is a marked geographical variation in the outgoing irradiance at the top of the atmosphere as well as in the net irradiance through the tropopause. The outgoing radiation is generally largest in the tropics because of the high surface temperatures, despite the fact that the trapping of the radiation also maximizes there due to the large gradient in temperatures between the surface and the tropopause. There is also a distinct longitudinal pattern where the role of clouds is dominant. Clouds very efficiently trap long wave radiation in the atmosphere, and as such contribute to the greenhouse effect.

The role of each of the climate gases and clouds for the greenhouse effect has been investigated. It is shown that clouds are responsible for about ¼ of the total greenhouse effect. Water vapour is by far the most important greenhouse gas, its contribution is about ½ of the total when clouds are also taken into account. On the global scale the contribution of ozone is modest, less than 3%.

Over the last decades there has been observed reductions in the stratospheric ozone concentrations, especially at high latitudes, as well as increased ozone concentrations in the troposphere over some geographical regions. The radiative effects of such changes have previously been investigated in a study by Shine et al. (1995). The calculations presented in this report are shown to compare very well with the results of this study.

Radiative impacts of ozone and other radiatively active components

1. Introduction

Ozone has a major influence on the radiative budget of the atmosphere. The control is mainly through its role in influencing the radiative balance, in the ultraviolet (UV) and visible as well as the infrared (IR) spectral regions. In the stratosphere, absorption of UV radiation by ozone in the ozone layer causes an increase in the temperature, e.g. by several tens of degrees near the stratopause. The impact on the tropospheric climate is more moderate, but the absorption of UV and visible radiation as well as the absorption and re-emission of IR energy plays a significant role in the energy balance of the troposphere.

Changes in stratospheric as well as tropospheric ozone have taken place over the last decades due to man made emissions. Stratospheric ozone has decreased since the end of the 1970'ies due to industrial production of chlorofluorocarbons (CFC's) and bromocarbons (Halons). Tropospheric ozone has increased considerably during the last century, presumably as a result of man made emissions of nitrogen oxides (NO_x), carbon monoxide (CO) and volatile organic compounds (VOC). The observed changes in ozone have undoubtedly had an impact on the radiative balance of the atmosphere.

In this work we investigated the roles of ozone in the climate system through its effects on the penetration of solar and terrestrial radiation in the atmosphere. Radiative transfer calculations have been performed under various assumptions for the vertical distribution of ozone as well as other parameters, such as temperature and water vapour content. A special emphasis has been on the conditions in the Nordic area, and ozone sonde profiles from 3 stations in this region have been used as a basis for radiative transfer calculations. Extrapolations to the global atmosphere have also been made, and in that case climatological data have been used for ozone and other greenhouse gases as well as for temperature and cloud distribution.

The tropospheric climate is governed by the net radiative irradiance through the tropopause, a quantity often called the radiative forcing. It defines the amount of radiative energy that is available for the earth- troposphere system. Much of the results and the discussion in this report is directed towards the understanding of the role of ozone in determining the radiative forcing.

As mentioned above, the temperature in the stratosphere is to a large degree determined by ozone. Any change in ozone therefore impacts the stratospheric temperatures. In order to make a realistic estimate of the radiative impact of changes in the ozone profile, it is necessary to allow the temperature to adjust to the altered ozone profile. In that case one denotes the estimated radiative forcing adjusted, whereas it is denoted instantaneous in the case when the temperature change is ignored.

A brief description of the radiative transfer codes used in this report for short wave as well as long wave radiation is given in section 2, along with a sensitivity test for vertical resolution of the long wave model. Based on ozone sonde results from 3 Nordic sites, seasonal cycles and trends have been investigated in the radiative forcing due to ozone both in the long wave and the short wave spectral regions. These results are presented in section 3. In section 4 a global climatology of radiative effects of ozone is presented. Such calculations have only been performed for the long wave radiation. This analysis includes an estimate of the role of ozone as compared to other greenhouse gases as well as clouds. Finally, in section 5, results from our models are compared to a previous study (Shine et al., 1995) where radiative effects of ozone changes were estimated by several models, taking long wave as well as short wave radiation into account.

2. Methods

Two radiative transfer models are used in this report. For the terrestrial infrared radiation a broad band model is used and a high resolution radiation model is used in the shortwave region.

2.1 Long wave radiation transfer model

The broad band model is developed at NILU and the University of Oslo (Stordal, 1988; Myhre and Stordal, 1995) and called the Oslo Broad band InfraRed (OBIR) model. The parameterization of the absorption due to ozone is based on work of Ramanathan and Dickinson (1976). Two ozone absorption bands in the infrared region are included . That is the main at 9.6 μm and the spectroscopically weaker band at 14 μm (Myhre and Stordal, 1995). Clouds are included in the OBIR model, where three cloud are used and random overlap between them are assumed. The three cloud layers can have variable emissivities. The OBIR model is compared to line-by-line (LBL) models in InterComparison of Radiation Codes used in Climate Models (ICRCCM) for clear sky cases and the major constitiuents in the infrared spectral region of the terrestrial radiation were included showing good agreement with the LBL models (Myhre and Stordal, 1995).

2.2 Short wave radiation transfer model

A spherical radiation model which is developed at the University of Tromsø and the University of Alaska (Dahlback and Stamnes, 1991; Dahlback et al., 1994) will be used for calculations in the UV and visible region. The model can easily be used at various degree of accuracy, by assuming scattering onto a varying number of spatial directions, treated in the model as stream directions. The model uses the DIScrete ORDinate method (DISORT). The spectral resolution for calculations in this report is 1 nm. The model has been widely used to study absorption by ozone, and modifications are currently being made to also aerosols.

2.3 Sensitivity of infrared radiative fluxes to vertical resolution

The modelled vertical distribution of infrared irradiances depends on the vertical resolution of the model. In this section this dependency is evaluated, and the choice of vertical resolution in the calculations presented in this report is thereby motivated.

The model has been run for five different vertical resolutions: 8, 15, 30, 60 and 120 levels. The top has been set at 30 km. Input data of ozone, water vapour and temperature has been based on ozone balloon soundings from Scoresbysund, Greenland. Three sonde profile types have been used: a smooth winter profile (from 1994-03-09), a smooth summer profile (1994-09-14) and an irregular winter profile (1995-03-24).

For each level and profile type the contribution from ozone has been determined in experiments where ozone has been the only absorber as well as in combination with CO_2 and H_2O taking overlap into account.

Ozone, temperature and water vapour data for the model layers have been derived from radiosonde observations, applying pressure-weighted integration.

The resolution sensitivity has been evaluated for the instantaneous radiative forcing. The forcing in the various experiments are compared to the forcing in the most accurate case (120 levels). The discrepancy at the tropopause level as well as at the level of the maximum discrepancy has been evaluated. Table 1 and Table 2 summarizes the results from the model runs.

The largest difference in radiative forcing due to ozone between the 120-level run and the 60-level run is 0.5%. The difference between the 120-level run and lower resolution runs is about the same for all three profile types *Winter irregular*, *Winter smooth* and *Summer smooth*. The largest difference in radiative forcing between the 120-level run and the 8-level run is 8.8%, occurring in the majority of cases, near the tropopause. The discrepancy is generally larger when overlap with CO_2 and H_2O is considered, but the overlap effect is moderate. It appears sufficient to run the radiative transfer model with a 60-level resolution. Even the 30- and 15-level cases have an acceptable accuracy for most purposes.

Table 1: Difference in radiative forcing due to ozone between 120-level run and lower resolution runs (60, 30, 15 and 8 levels). Ozone has been assumed to be the only absorber.

	Difference in F_{net} between 120-level run and N-level run			
	N=60	N=30	N=15	N=8
Winter irregular				
At tropopause (h = 8.2 km)	0.01%	0.5%	0.9%	2.4%
At level of max. difference	0.5%	1.2%	1.9%	4.6%
Level of max. difference	7.2 km	8.7 km	10.7 km	12.0 km
Winter smooth				
At tropopause (h = 8.8 km)	0.03%	0.2%	0.9%	4.1%
At level of max. difference	0.5%	1.1%	3.2%	7.1%
Level of max. difference	9.0 km	9.5 km	10.5 km	11.7 km
Summer smooth				
At tropopause (h =11.1 km)	0.3%	1.0%	2.4%	8.1%
At level of max. difference	0.5%	1.6%	3.5%	8.1%
Level of max. difference	11.6 km	12.1 km	13.1 km	12.4 km

Table 2: Difference in radiative forcing due to ozone between 120-level run and lower resolution runs (60, 30, 15 and 8 levels). Ozone has been considered in combination with CO_2 and H_2O.

	Difference in F_{net} between 120-level run and N-level run			
	N=60	N=30	N=15	N=8
Winter irregular				
At tropopause (h = 8.2 km)	0.1%	0.5%	1.1%	2.4%
At level of max. difference	0.5%	1.4%	2.1%	4.7%
Level of max. difference	8.7 km	8.7 km	4.6 km	12.0 km
Winter smooth				
At tropopause (h = 8.8 km)	0.003%	0.1%	0.7%	4.3%
At level of max. difference	0.5%	1.3%	3.4%	7.4%
Level of max. difference	9.0 km	9.5 km	10.5 km	11.7 km
Summer smooth				
At tropopause (h =11.1 km)	0.3%	1.1%	2.6%	8.8%
At level of max. difference	0.5%	1.7%	3.6%	8.8%
Level of max. difference	11.6 km	12.1 km	13.0 km	12.4 km

3. Trends and seasonal variations at three Nordic stations

In the following we have estimated the radiative forcing due to ozone at the three sonde stations Gardermoen, Sodankylä and Scoresbysund. Calculations have been performed for infrared radiation of all the stations, whereas calculations of transfer of solar radiation has been performed at Gardermoen only. Observed ozone, temperature and water vapour have been used as model input, and all sonde data in the period January 1991–June 1995 (Sodankylä from February 1989) have been used. We have focused our study on seasonal variations and long term trends.

3.1 Long wave radiation

The OBIR model has been run with a vertical resolution of 60 levels. The top level was chosen at 10 mbar (about 30 km). Only profiles with data up to the 10 mbar level have been included. For each sonde profile the radiative forcing due to ozone has been calculated, taking overlap with CO_2 and H_2O into account.

The temperature and water vapour concentration both influence ozone's radiative forcing effect. In the following we present results for the seasonal variation in the ozone forcing. It is clear that this is influenced not only by the variation in ozone itself, but also by the variation in temperature and water vapour. The part of the seasonal variation in the forcing that is due to the concentration of ozone itself has been estimated by performing control runs with constant temperature and water vapour.

Figure 1a shows the calculated radiative forcing at Gardermoen for the period 1991–95 based on sonde measurements of ozone, temperature and water vapour. Based on these values monthly mean values have been calculated and are presented in Figure 1b. The average radiative forcing over the time period studied is 3.5 W/m^2 at the tropopause and 7.8 W/m^2 at the top of the atmosphere.

Figure 1c shows the forcing based on the same ozone sonde data, but using an average summer temperature and water vapour profile for the whole data series. Figure 1d shows monthly averages for these data. Finally, Figure 1e shows the forcing based on winter average temperature and water vapour profile with monthly averages illustrated in Figure 1f.

The results for Sodankylä and Scoresbysund are shown in Figures 2 and 3, respectively. The average radiative forcing over the time periods studied is 3.6 W/m^2 and 3.2 W/m^2 at Sodankylä and Scoresbysund, respectively, at the tropopause level. The corresponding numbers for the top of the atmosphere are 7.3 W/m^2 and 5.5 W/m^2.

There is a clear seasonal variation in the radiative forcing due to ozone at all stations. It shows maximum values in the summer and minimum values in the winter.

When the same temperature and water vapour profiles are used throughout the time series the seasonal variation is reduced considerably, as the winter forcing is increased whereas the summer forcing is reduced.

It is difficult to observe any clear trends in radiative forcing between 1991–1995, mainly due to the short time period and the relatively limited number of ozone profiles. We can, however, see a slight increase at Gardermoen for the months December, January and February throughout the period. From this analysis we cannot conclude whether this is due to changes in stratospheric or tropospheric ozone. Clearly, more sonde data are necessary in order to establish long term trends in the forcing.

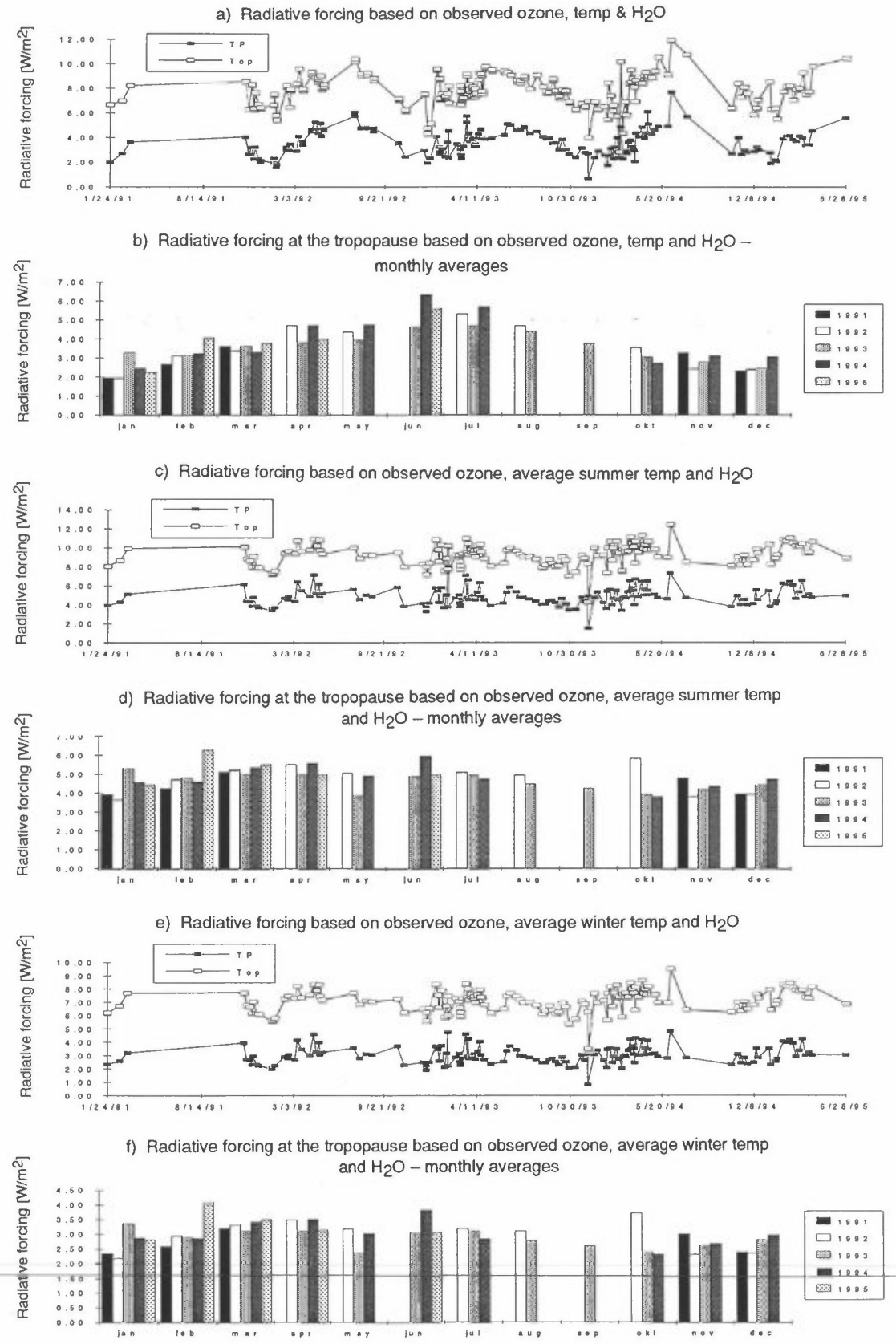

Figure 1: The contribution to radiative forcing due to ozone based on sonde measurements at Gardermoen 1991-95. Results are given for the tropopause (Tp) level as well as for the top of the atmosphere (Top).

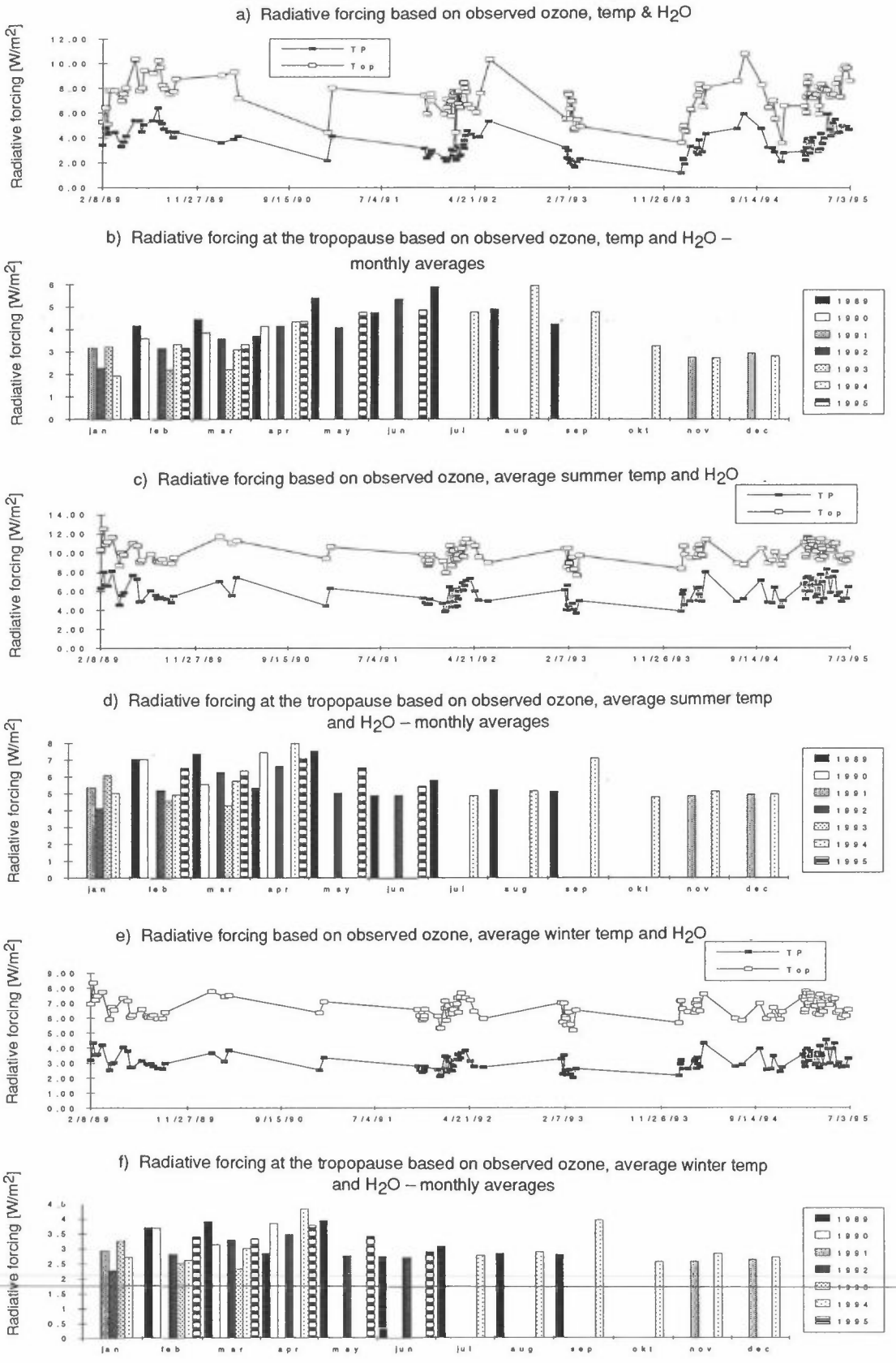

Figure 2: The contribution to radiative forcing due to ozone based on sonde measurements at Gardermoen 1991-95. Results are given for the tropopause (Tp) level as well as for the top of the atmosphere (Top).

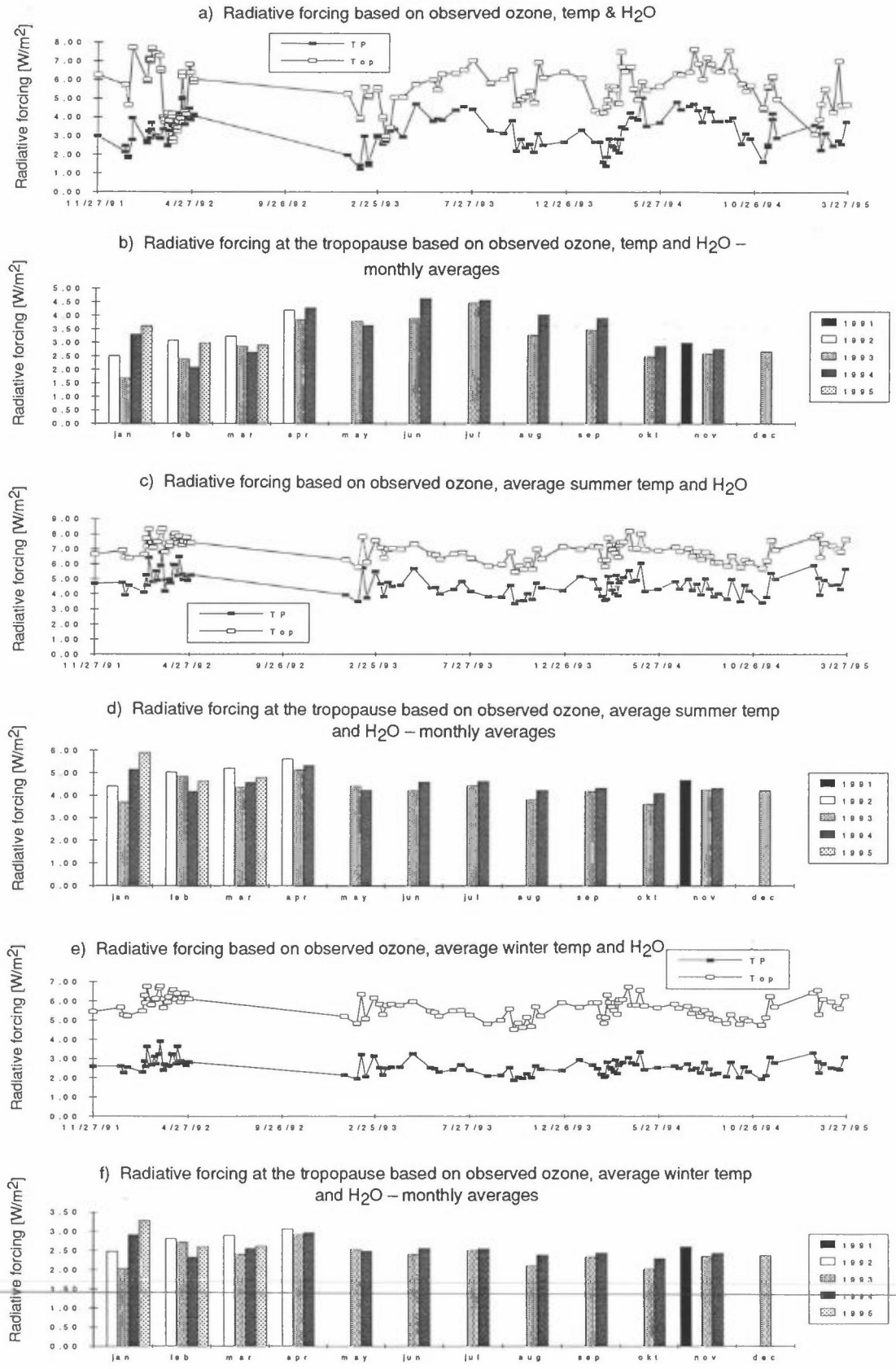

Figure 3: The contribution to radiative forcing due to ozone based on sonde measurements at Gardermoen 1991-95. Results are given for the tropopause (Tp) level as well as for the top of the atmosphere (Top).

3.1.1 *The role of temperature and humidity*

Above we have seen that the temperature and water vapour content are important in the seasonal cycle of the radiative forcing due to ozone. In the following the roles of each of these factors are studied. Additional runs have been performed when the temperature alone as well as the water vapour alone has been kept constant at summer average values. The results are shown in Figure 4 for 1992. Compared to the case that includes seasonal variation of all parameters, the case with constant temperature and water vapour differs by 46% as a yearly average, whereas the cases with either temperature or water vapour fixed differ by 44% and 10% respectively, clearly underlining the strong role of the temperature. The results in Figure 4 shows that the seasonal cycle of the radiative forcing due to ozone as well as its average value depend strongly on the temperature.

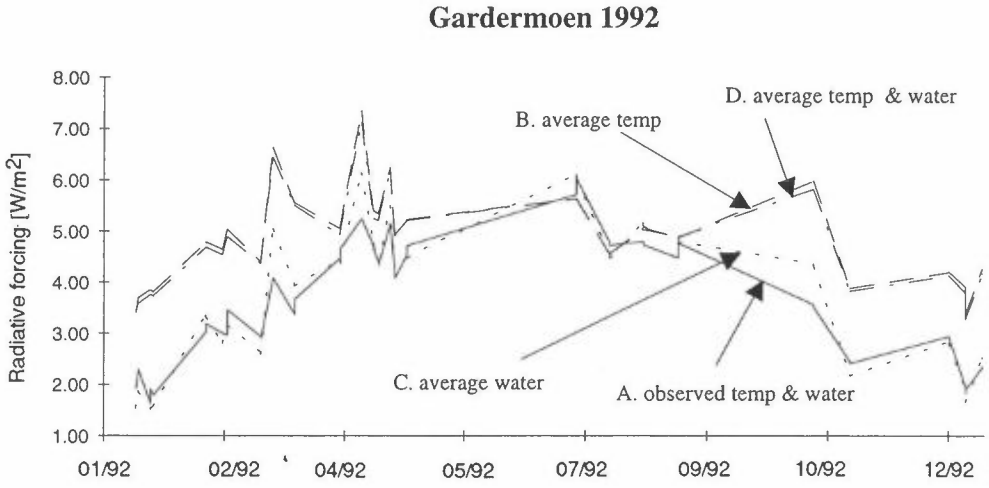

Figure 4: Radiative forcing at Gardermoen for four cases. Case A is based on observed temperature and water vapour, case B is based on an average summer temperature profile, case C is based on an average summer water vapour profile and case D is based on average summer temperature and water vapour profiles. Results are for the tropopause level.

3.1.2 *The role of overlap from CO_2 and H_2O*

In order to study the effect of overlap from CO_2 and water vapour on the radiative forcing due to O_3 two test cases have been run on the Gardermoen series. As in section 2.3, this has been done by including as well as excluding the overlap in the calculations. Figure 5 shows results for the two cases. The average difference between the two cases over the study period 1991–1995 is 17% at the tropopause and 19% at the top of the atmosphere.

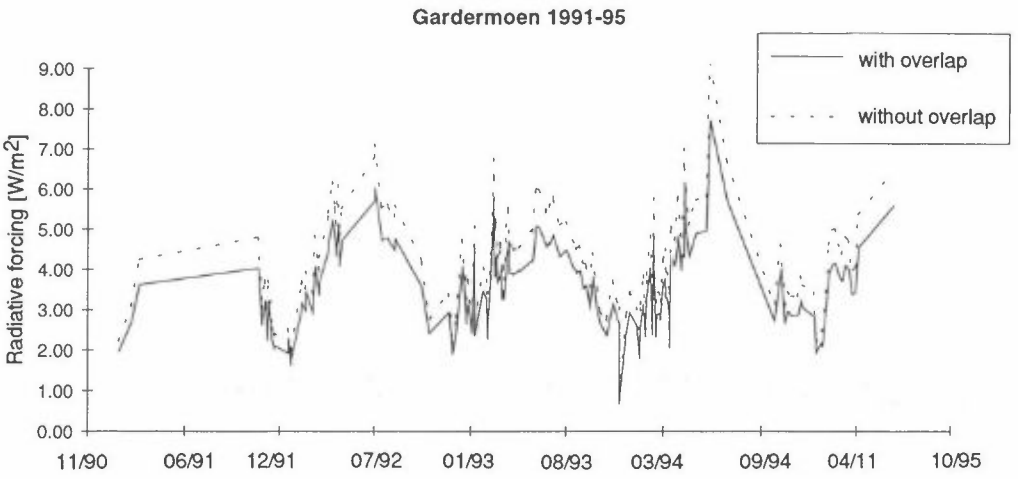

Figure 5: Radiative forcing due to ozone, including and excluding overlap. Results are for the tropopause level.

3.2 Short wave radiation

In this section we present results of short wave radiative transfer calculations. Vertical profiles of ozone and temperature are taken from ozone soundings, and calculations are made for the Gardermoen station. A total of 176 sonde ascents have been found appropriate for the analysis.

For short wave calculations it is important to include also the upper stratosphere. Constant ozone mixing ratio has been applied to the levels above the level where the sonde balloon has exploded and up to the top level at 60 km. The temperatures of these levels have been calculated from the top sonde level and standard stratospheric lapse rate. The pressure is set as standard atmosphere pressure. These approximations are believed to reflect atmospheric conditions with satisfactory accuracy.

The analysis shows the instantaneous radiative forcing of ozone at tropopause level. It has been performed twice with constant zenith angle. The first analysis was made with an albedo that varies according to typical seasonal conditions at Gardermoen based on satellite data from International Satellite Cloud Climatology Project (ISCCP) (Rossow and Schiffer, 1991) and the second was using a fixed albedo of 0.2, which is assumed to represent an average annual value.

A third calculation has been performed to include the effect of seasonal variations of the zenith angle. For simplicity an average zenith angle has been used for each month.

Figure 6 shows the radiative forcing due to ozone at Gardermoen in the period 1991–1995 under the assumption of a seasonably varying albedo. The average value of the 176 sonde ascents has been found to be 10.4 W/m^2. Most values are located between 8 W/m^2 and 12 W/m^2 with a maximum forcing of 14.5 W/m^2 at April 6th 1994 and a minimum forcing of only 6.1 W/m^2 at January 15th 1992.

It is worth noticing that the sonde ascents are quite sparsely distributed during the summer months compared to the rest of the year. This reduces the reliability of the analysis of the summer period, but even when this is taken into consideration it is not possible to see any distinct temporal trends in the forcing from this figure.

Monthly mean values of the radiative forcing are also shown in Figure 6. There is a marked seasonal variation. Due to high ozone amounts the forcing reaches its highest values during the spring with a peak in April. The lowest values occur in the winter when ozone values are slightly lower than spring values and the snow cover gives a high albedo. The summer and autumn values seem to be located somewhere between the winter values and the spring values but generally closer to the latter.

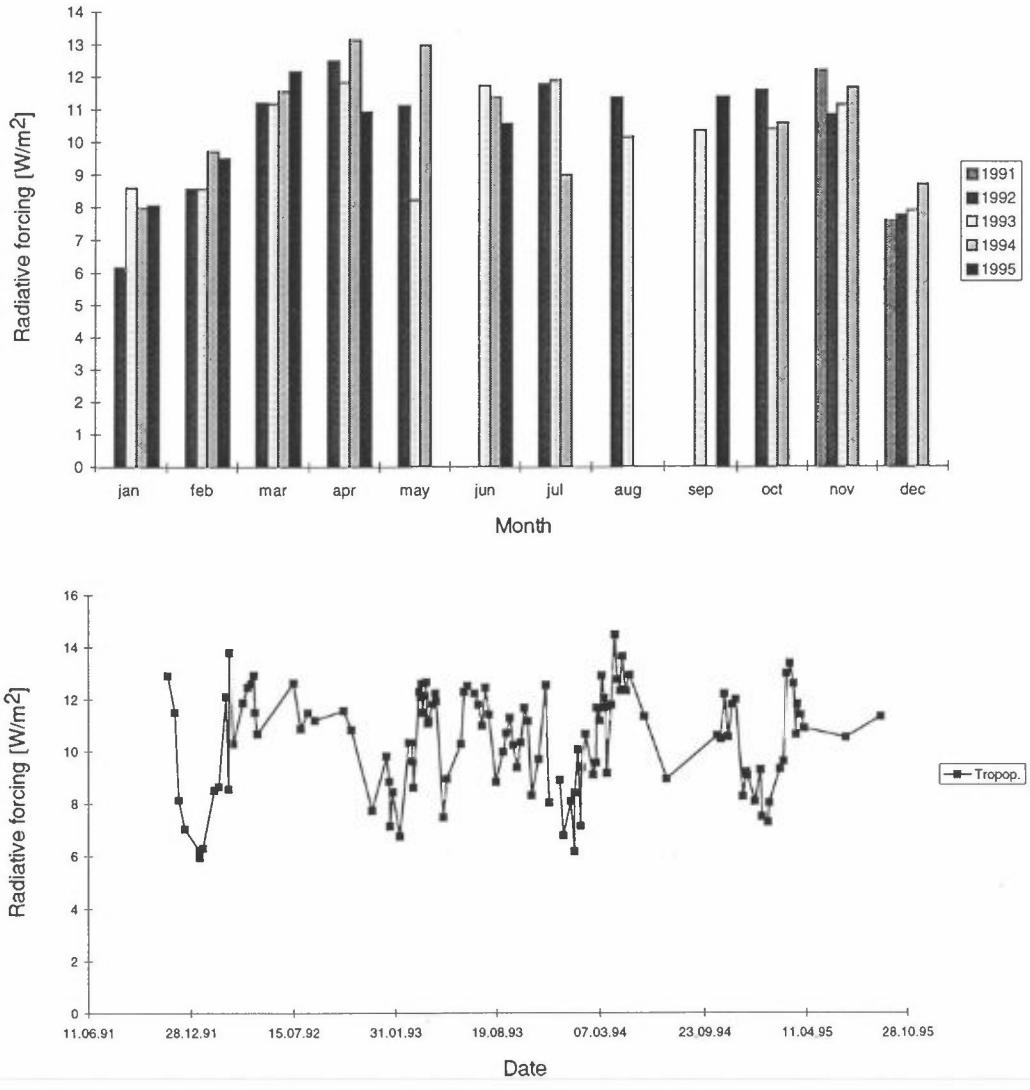

Figure 6: Short wave radiative forcing due to ozone at the tropopause level. The results are based on ozone soundings at Gardermoen. The upper panel shows monthly averages, wheras individual values are given in the lower panel. The albedo is varied over the year, and the zenith angle is held fixed.

Figure 7 shows the radiative forcing due to ozone when the albedo is held constant. The mean value in the case of a constant albedo of 0.2 is 11.7 W/m^2 with most values concentrated between 9 W/m^2 and 14 W/m^2. The forcing due to ozone reaches a maximum value of 15.5 W/m^2 at March 13th 1992 and a minimum of 7.9 W/m^2 at October 27th 1993.

The monthly means of the radiative forcing are also given in Figure 7. The figure shows more distinctly that the forcing of ozone is closely related to the annual cycle of the amount of ozone in the atmosphere. Due to the pattern of ozone transportation the maximum values at Gardermoen occur during spring. Minimum amounts are obtained in late summer and early autumn with a gradual build-up during the winter. As can be seen from this figure the ozone forcing follows the same pattern.

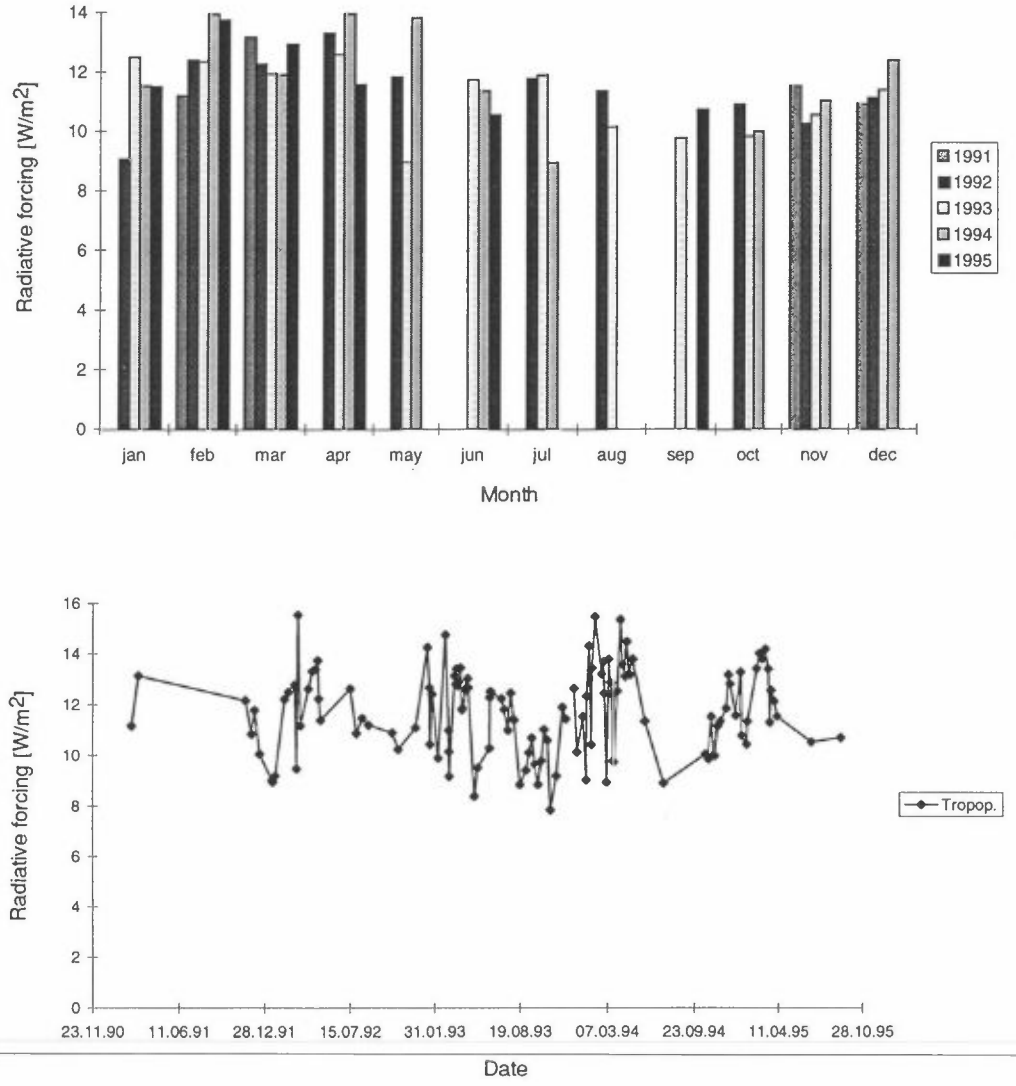

Figure 7: Short wave radiative forcing due to ozone at the tropopause level. The results are based on ozone soundings at Gardermoen. The upper panel shows monthly averages, wheras individual values are given in the lower panel. The albedo is held constant at 0.2, and the zenith angle is held fixed.

Figure 8 shows the radiative forcing due to ozone when the albedo is held fixed at 0.2 and the zenith angle is allowed to vary according to its seasonal values. In this case the mean value has been found to be 11.3 W/m2. The minimum value of 4.6 W/m2 occurs at December 8th 1993 and the maximum value of 18.9 W/m2 at May 4th 1994.

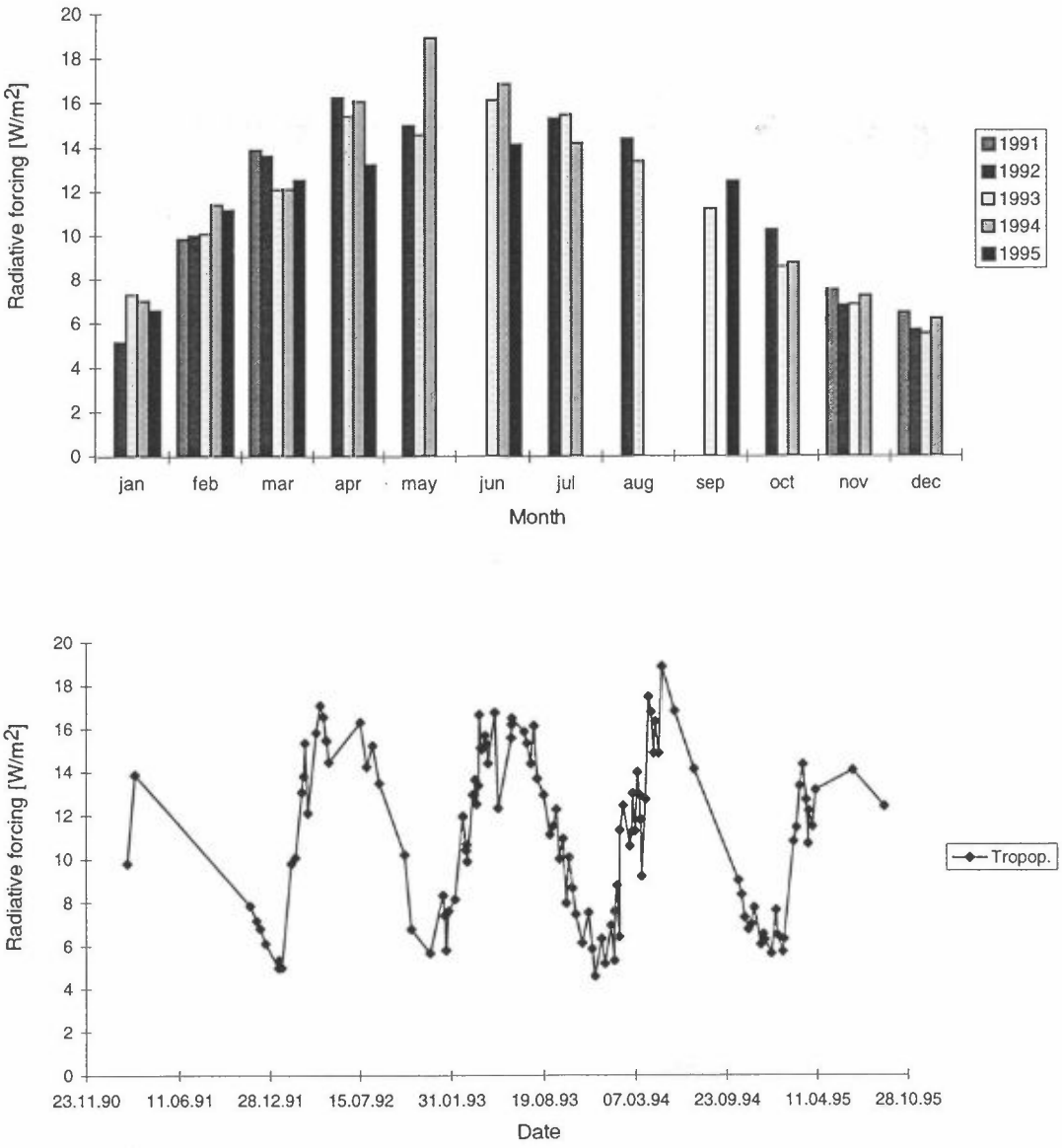

Figure 8: Short wave radiative forcing due to ozone at the tropopause level. The results are based on ozone soundings at Gardermoen. The upper panel shows monthly averages, wheras individual values are given in the lower panel. The albedo is held constant at 0.2, and the zenith angle is varied according to seasonal values.

One striking feature when comparing this figure to Figures 6 and 7 is that the extremes have been much more accentuated with higher values in the summer season and lower values in the winter. A comparison between the two calculations

determining the radiative forcing due to ozone. Due to the high latitude of Gardermoen the station experiences a considerable variation in insulation between summer and winter and this gives rise to an amplification of the seasonal variation in radiative forcing of ozone.

The seasonal cycle showed in Figure 8 displays this pattern even more clearly. The maximum values occur in late spring and early summer when the ozone amount is still relatively high and the sun rises high in the sky. The minimum values can be found near the winter solstice when the insulation at Gardermoen is very low. The available short wave radiation to be absorbed at this time of the year has a low intensity.

4. Global climatology of infrared radiative forcing

Long wave radiation is trapped in the atmosphere by clouds as well as by water vapour, ozone, and the well mixed greenhouse gases as CO_2, CH_4, N_2O, and halocarbons. At the top of the atmosphere (TOA) there exists a balance between the global average outgoing long wave radiation (OLR) and the incoming short wave radiation. However there is large regional variation in the outgoing long wave radiation, as it is for the incoming short wave radiation. Particularly large are the latitudinal variations, but also longitudinal variations in the OLR are marked. As ozone varies with longitude, latitude, and altitude, the radiation trapped by ozone shows regional variation. We will in the following focus on the radiative forcing due to ozone, but of importance for the radiative forcing due to ozone is also the available radiation, and thus it is important to study the radiative forcing due to clouds and the other gases that also trap radiation in the atmosphere.

The OBIR model is used to calculate long wave radiative fluxes as a function of latitude, longitude, and altitude based on climatological data. The data for temperature and water vapour are from the European Centre for Medium-Range Weather Forecasts (ECMWF) as monthly mean data. The ozone data are climatological data based on satellite and sonde observations (Liang and Wang, 1995). Cloud data are taken from the International Satellite Cloud and Climatological Project (ISCCP, Rossow and Schiffer, 1991). For the well mixed greenhouse gases the IPCC (1994) mixing ratios are used. The horizontal resolution of the model is 2.5 deg*2.5 deg. In the vertical, 25 layers are used, where 16 of these are at the same levels as the ECMWF data. Near the tropopause 7 layers are included to give a better representation of the ozone in this altitude region. The data from ECMWF have values up to 10 mb, and we have included two higher levels in the radiative calculations; at 5 and 2.5 mb, where the temperatures have been increased by 10 and 20 K respectively compared to the 10 mb level.

4.1 Results at the top of the atmosphere

There has lately been an increased interest in the TOA fluxes, because of the possibility to measure fluxes at TOA by satellites, e.g. the Earth Radiation Budget Experiment (ERBE, Ramanathan et al., 1989). The measurements have the

possibility to observe both the global distributions of the OLR at TOA and the global distribution of the clear sky TOA fluxes.

Figure 9 shows the OLR at TOA as a yearly average and as a function of latitude and longitude as calculated by the OBIR model. The OLR at TOA shows large latitudinal variations from 120 W/m^2 at high latitudes in the Southern hemisphere and about 160 W/m^2 at high latitudes in Northern hemisphere, to 300 W/m^2 at low latitudes. Generally the OLR is somewhat lower near the equator than at 10-20 degrees in both hemispheres. Also longitudinal variations are marked, especially over land. The radiation emitted from the TOA can be seen to depend strongly on the surface temperature. E.g., the low values over the Himalayas reflect the low surface temperature in this region.

Figure 10 shows the radiation that is trapped in the atmosphere by greenhouse gases and clouds from the surface to the TOA. There is a somewhat larger regional variation in the trapped radiation than in the outgoing radiation. The highest values are near the Inter Tropical Convergence Zone (ITCZ). In Antarctica some regions with negative values are identified. This is due to a strong temperature inversion, so that more radiation can be emitted at TOA than at the surface. The calculated global yearly average of the radiation trapped by the atmosphere is 152.2 W/m^2.

Trapping of the radiation is due to the greenhouse gases (CO_2, water vapour, ozone, CH_4, N_2O, and halocarbons) and clouds. The temperature is responsible for most of the latitudinal variations shown in the two previous figures. Satellites have the possibility to measure both clear sky fluxes and the OLR. The difference between clear sky radiative fluxes and the OLR is then the radiative forcing due to clouds, called Cloud Radiative Forcing (CRF).

Figure 11 shows the yearly average cloud radiative forcing calculated by the OBIR model. The regional variations are relatively large, with the highest values of CRF near the ITCZ and the regions between 30-60 degrees in both the Southern and the Northern Hemisphere. Longitudinal variations are found particularly in the regions with high CRF, and the longitudinal variation mainly reflects a land/sea variation. This is especially marked near the ITCZ. The global average of the CRF is 20.5 W/m^2 with values up to 70 W/m^2 near equator and negative values in Antarctica due to the temperature inversion. Low values of CRF are also located near the subtropical high pressure regions, where there are small amounts of clouds. The high clouds are mostly responsible for the high values of CRF.

The calculated global mean of CRF, 20.5 W/m^2, is lower than the ERBE value; 31.1 W/m^2. The OLR at TOA calculated by the OBIR model and the observation from ERBE is 240.3 W/m^2 and 234.5 W/m^2 respectively. However the regional pattern of CRF is in much better agreement with the ERBE data. One reason for the discrepancy between the levels of observed and the modelled CRF could be that the ERBE clear sky emitted long wave radiation at the TOA can be overestimated (Harrison et al., 1990; Hartman et al., 1992). The uncertainties in the CRF calculated with the OBIR model are the radiation scheme, the fact that there has been assumed unit emissivity at the surface, and the input data used for

temperature, water vapour, and cloud data. The radiation scheme is earlier tested (Myhre and Stordal, 1995) to be inside the variations among various Line By Line models used in the InterComparison of Radiation Codes used in Climate Models (ICRCCM). Another satellite observation, NIMBUS-7 (Ardanuy et al., 1991), observed a CRF of 24.1 W/m^2 and the emitted long wave clear sky radiation at the TOA of 259.3 W/m^2. Rossow and Zhang (1995) have calculated top of atmosphere radiative fluxes from physical quantities based on the ISCCP data set with an annual global average CRF of 21.3 W/m^2 and OLR 234.2 W/m^2.

Table 3 summarizes the results from the two satellites, the calculated fluxes based on the ISCCP data set, and the results calculated with the OBIR model based on ECMWF and ISCCP data.

Table 3: Outgoing long wave radiation, emitted long wave clear sky radiation, and cloud radiative forcing at the top of the atmosphere from four different works.

Source	Outgoing long wave radiation	Emitted long wave clear sky radiation	Cloud radiative forcing
ERBE (Ramanathan et al., 1989)	234.5	265.6	31.1
Nimbus 7 (Ardanuy et al., 1991)	235.2	259.3	24.1
Rossow and Zhang (1995)	234.2	255.5	21.3
This work	242.3	262.8	20.5

In the following we present estimates of the contribution of ozone in the radiative budget of the atmosphere. Calculations have been performed with and without ozone included. We have used the observed temperatures in both cases, although the temperatures would have been different in an atmosphere without ozone. When the assumption of constant temperatures is used, one usually denotes the forcing as instantaneous.

The yearly average radiative forcing due to ozone at TOA is shown in Figure 12. The global yearly average is 6.00 W/m^2. The highest values have been estimated over Northern Africa. Negative values are found in Antarctica also in this case due to the temperature inversion. In order to quantify the effect of clouds on the contribution of ozone to the trapping of long wave radiation, experiments with and without ozone have been made also for clear sky conditions. Without clouds the radiative forcing at TOA is increased to 8.32 W/m^2, which is an increase by 39%. The radiative forcing due to ozone when clouds are included is reduced in regions with high CRF, where less irradiance is available to absorb. This is marked near equator. The cloud effect shows clear longitudinal variations which mirrors the trapping of the radiation by the clouds.

4.2 Results at the tropopause

Radiative fluxes at the tropopause level are of particular importance, as they define the energy that is available for the troposphere/Earth system, which

determines the weather and to a large extent the climate. Unlike the TOA fluxes, the tropopause fluxes cannot be detected by satellite instruments, making verification of the model calculation more difficult.

Figure 13 shows the radiative forcing due to ozone at the tropopause level. The picture is different from the forcing at TOA. Large values are estimated near 30 deg in both hemispheres. The radiative forcing is stronger at TOA than at the tropopause, in particular at low latitudes. Regions with high values of the CRF give smaller values of the radiative forcing due to ozone at the tropopause level, as was also the case at TOA. The global yearly average radiative forcing at the tropopause is calculated to 3.38 W/m^2 and 3.96 W/m^2, with and without clouds respectively, a difference of 17%. Clouds more efficiently reduce the radiative forcing due to ozone at TOA than at the tropopause.

In Figures 14 and 15 the radiative forcing due to tropospheric and stratospheric ozone is shown for the tropopause level. The pattern of the forcing due to tropospheric ozone largely resembles the pattern of the total forcing, although the values are somewhat smaller. The forcing due to tropospheric ozone is much lower at high latitudes, where the forcing due to stratospheric ozone maximize. The relatively weak forcing due to stratospheric ozone in equatorial regions is due to the fact that the tropopause is high and cold in this region. The global yearly average radiative forcing due to the tropospheric ozone is 1.42 W/m^2 and the radiative forcing due to the stratospheric ozone is 1.96 W/m^2. The difference between the radiative forcing due to ozone at TOA and at tropopause is due to the higher absorption by ozone upward than downward in the stratosphere.

The tropopause level varies with latitude, and is highest over equator. In the analyses presented in this section, the tropopause level is chosen where the temperature gradient changes sign, except at high latitudes where the temperature gradient is weak over a substantial height region and the tropopause level is chosen so that a weak negative gradient is allowed even above the tropopause (typically 8–10 km). The radiative forcing due to ozone is not very dependent upon the temperature at the tropopause level. A decrease of the temperature of 2 K in the tropopause level gives a decrease of the radiative forcing due to ozone of 0.15%. On the other hand the radiative forcing due to ozone depends upon the height of the tropopause. If the level of analyses is increased one level higher up (to 25 mb lower pressure) the radiative forcing due to ozone increases to 3.64 W/m^2, or by 8%. The total radiative flux at the tropopause varies less with the tropopause level, indicating that the level which is chosen for analyses is especially important for the radiative forcing due to ozone. If this level is decreased to one level lower (to 25 mb higher pressure) the radiative forcing due to ozone decreases to 3.13 W/m^2, or a 7% decrease. It is especially the upward radiation that is responsible for the variation between various levels.

As will be described in more detail in section 5, two bands of ozone are of importance in the infrared region. The main band is centred in the atmospheric window region near 9.6 μm. A spectroscopically weaker band which is located at 14 μm, is more strongly overlapped with other gases. Out of the radiative forcing due to ozone of 3.38 W/m^2 the 14 μm band of ozone is responsible for 0.416 W/m^2 or 12%. When clouds are not taken into account the radiative forcing

due to the 14 μm of ozone is only increased to 0.422 W/m^2 whereas the total radiative forcing due to ozone is increased, as earlier mentioned, to 3.96 W/m^2. While the radiative forcing due to ozone is distributed relatively evenly between the tropospheric and stratospheric contribution for the 9.6 μm band, the stratospheric contribution is dominating for the 14 μm band.

The ozone climatology is based on satellite and sonde observation, and gives mostly latitudinal variations. The data are given as monthly averages, and longitudinal gradients are therefore smoothed out to a large extent. However in the winter period in the Northern hemisphere marked longitudinal variations were present.

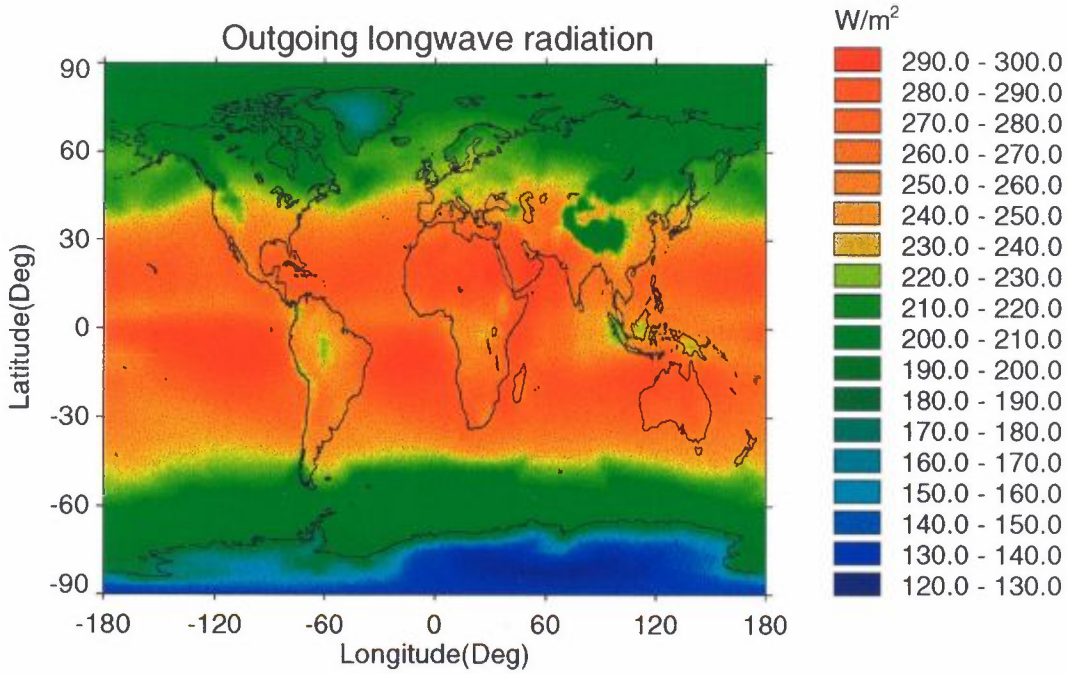

Figure 9: Yearly average outgoing longwave radiation at the top of the atmosphere given in W/m².

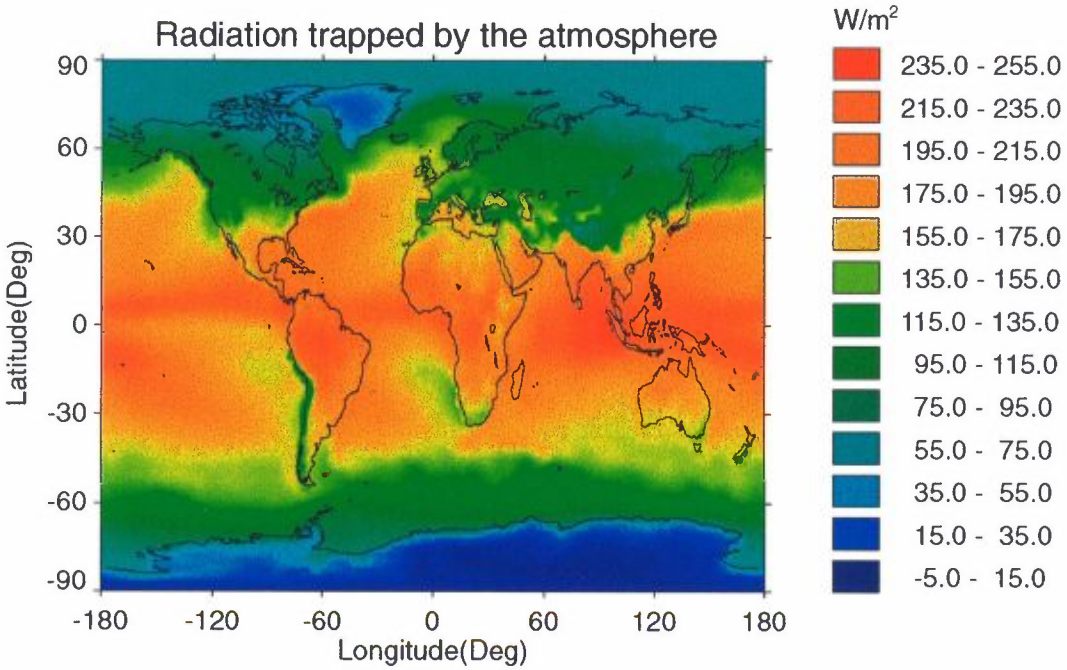

Figure 10: Yearly average radiation trapped by the atmosphere given in W/m².

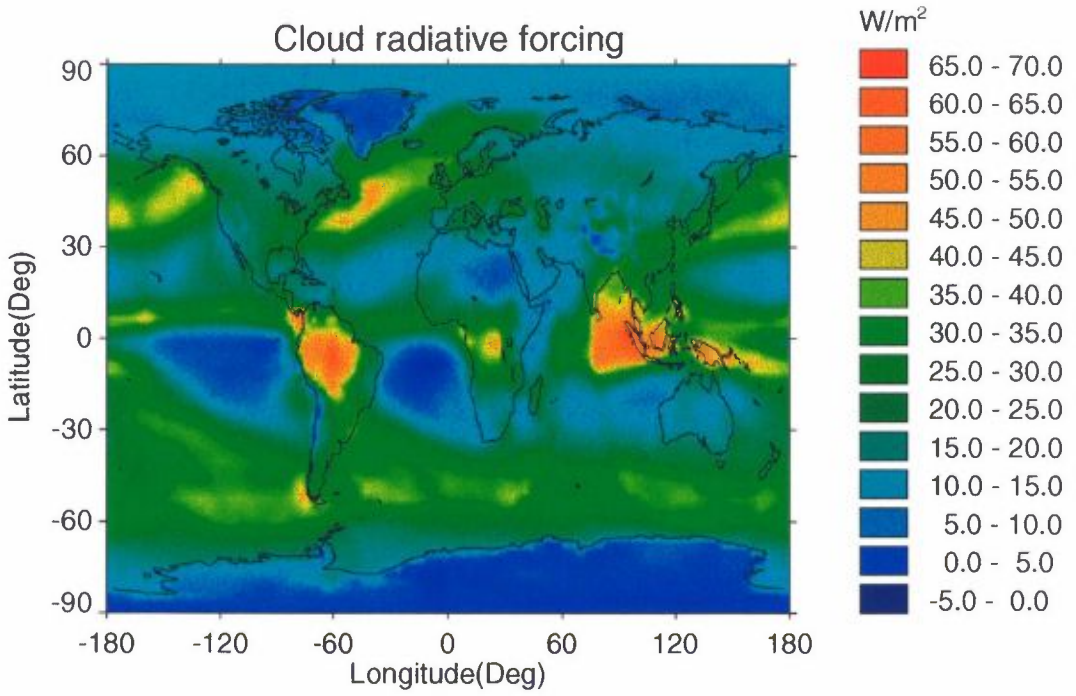

Figure 11: Yearly average cloud radiative forcing at the top of the atmosphere given in W/m². Clouds data from ISCCP.

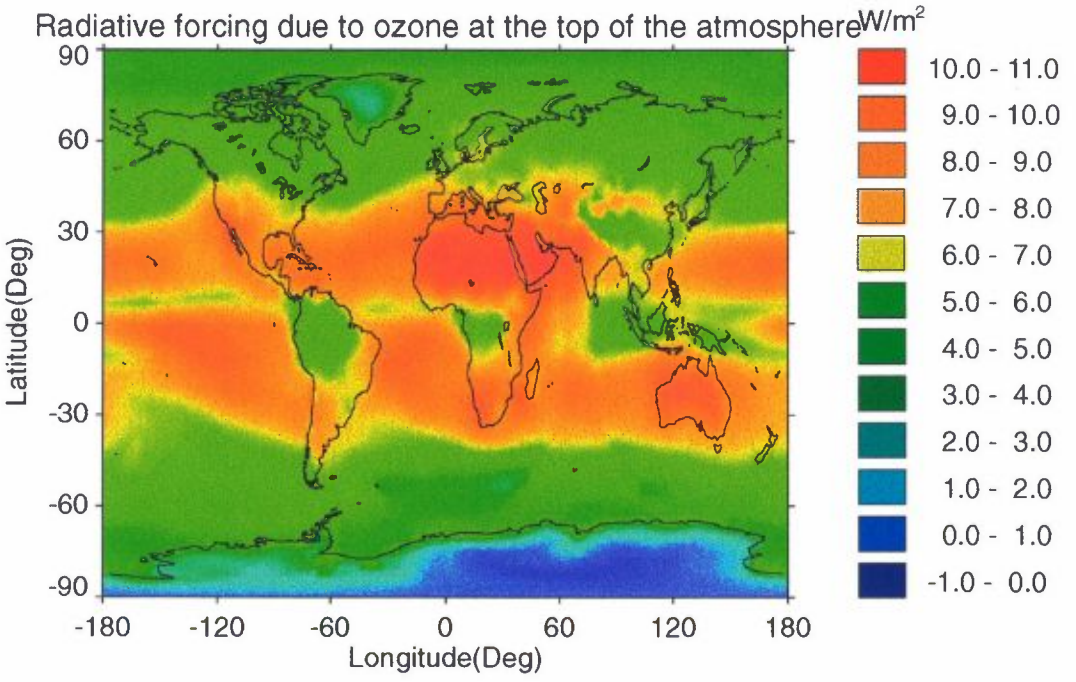

Figure 12: Yearly average radiative forcing due to ozone at the top of the atmosphere given in W/m².

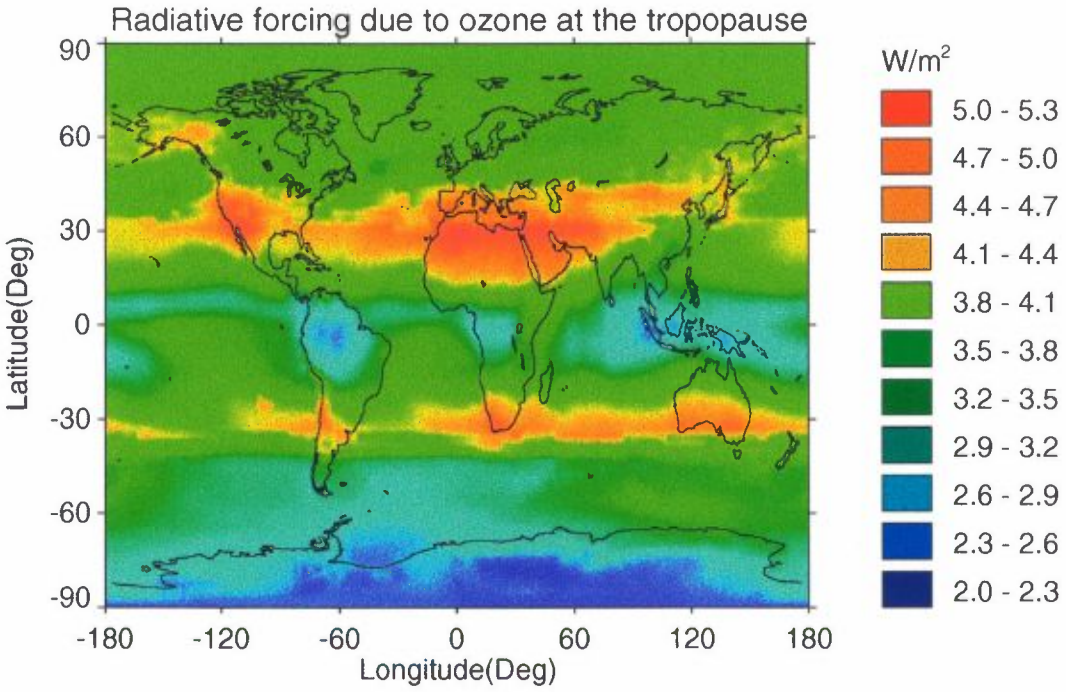

Figure 13: Yearly average radiative forcing due to ozone at the tropopause given in W/m².

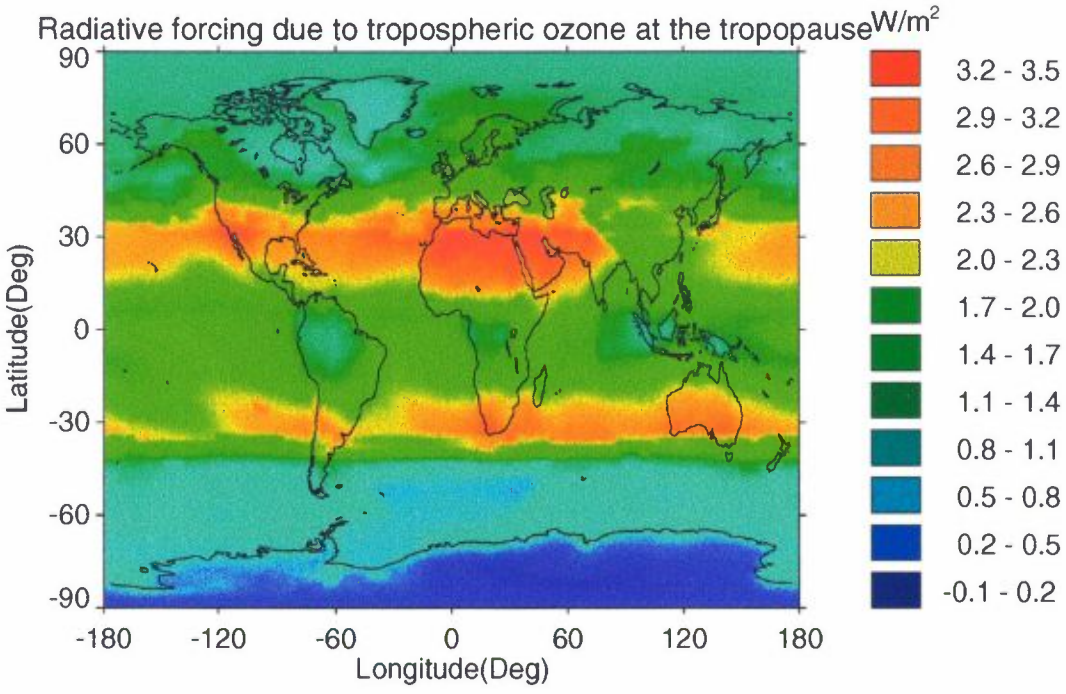

Figure 14: Yearly average radiative forcing due to tropospheric ozone at the tropopause given in W/m².

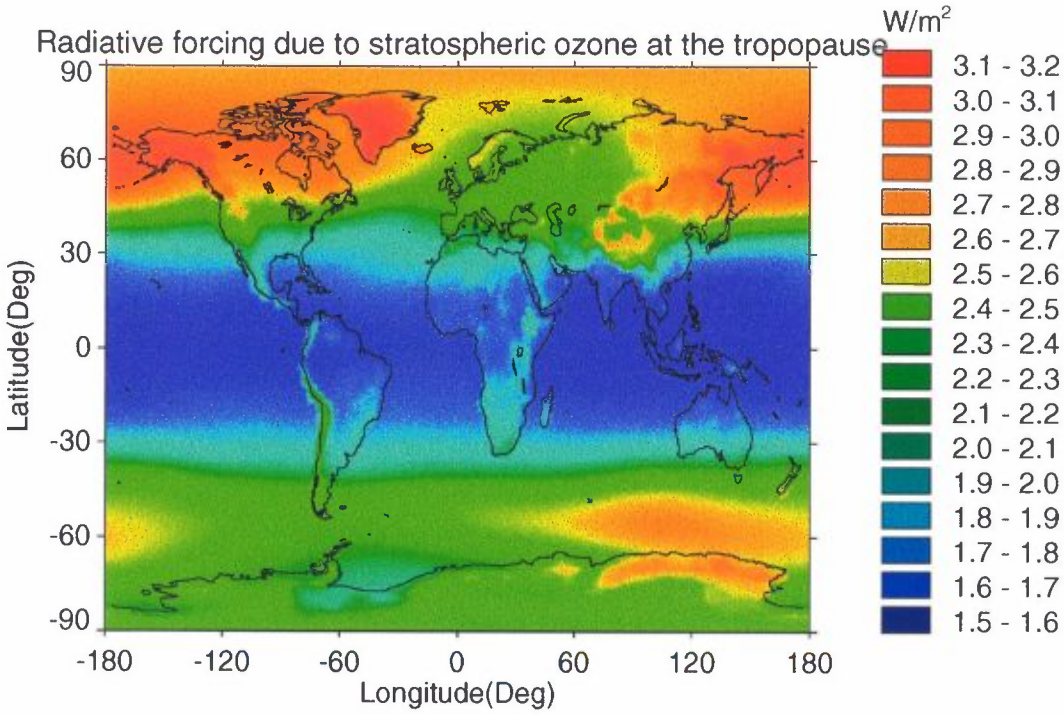

Figure 15: Yearly average radiative forcing due to stratospheric ozone at the tropopause given in W/m².

4.3 The role of ozone compared to other infrared active species

In the following we will estimate the relative contribution of each of the components to the total radiative forcing at the tropopause, and we start with considering only the three major contributors in the present atmosphere – H_2O, CO_2 and clouds. Table 4 shows the radiative forcing from each of the three components and mixtures of them. Overlap effects are also shown.

Table 4: Radiative forcing and overlap effect at the tropopause for different mixtures of the components H_2O, CO_2, and clouds. Values are given in W/m² and represent global, yearly averages.

Components	Radiative forcing	Overlap effect
H_2O	100.5	
CO_2	50.4	
Clouds	61.3	
H_2O and CO_2	138.4	12.4
H_2O and clouds	129.6	32.2
CO_2 and clouds	101.1	10.6
H_2O, CO_2, and clouds	162.1	50.0

The total radiative forcing for these three components is 162.1 W/m² and the overlap is 50.0 W/m². Most easily, the relative contribution can be found when considering three independent experiments with only one of the components present and scaling the contribution to add up to 162.1 W/m². Results of such considerations are given in Table 5, denoted as method 1. In the real atmosphere, however, all three components act simultaneously. Since the components overlap it is not trivial to estimate the relative effects of each of the components, since there are in principle many ways to take overlap effects into account.

Table 5: Distribution of the radiative forcing in W/m² of H_2O, CO_2, and clouds for three different methods.

Method	H_2O	CO_2	Clouds
Method 1	76.8 (47.4%)	38.5 (23.7%)	46.8 (28.9%)
Method 2	79.7 (49.2%)	40.9 (25.2%)	41.5 (25.6%)
Method 3	80.1 (49.4%)	40.3 (24.9%)	41.7 (25.7%)

Table 6 shows the overlap between first two of the components (already shown in Table 4) and then overlap when the third component is added. In all three cases the total overlap is 50.0 W/m².

Table 6: The overlap effect when first a mixture of two components is present, and then adding the third component. All values are in W/m².

Mixture of two components		Adding the third component		Total overlap
H_2O and CO_2	12.4	+ clouds	37.6	50.0
H_2O and clouds	32.2	+ CO_2	17.8	50.0
CO_2 and clouds	10.6	+ H_2O	39.4	50.0
Total	55.2	Total	94.9	

The total reduction in radiative forcing that is obtained when all three components are present, can be allocated to each of the individual components in several ways. Allocation by distribution of the reduction proportionally to the radiative forcing from each component, would give the same results as in the method 1 above. The reduction of the individual radiative forcing of each of the components due to the combined overlap between them can be handled using the information on the overlap between the components. First, the overlap when the third component is added to the two others, as shown in column two in Table 5. This overlap is used and scaled to the total overlap of 50.0 W/m². This method is denoted as method 2, and results are shown in Table 6. Alternatively, the overlap effect for only two components can be considered in addition to the overlap in method 2, referred to as method 3 in Table 6. I.e. in method 3, the overlap effect of e.g. H_2O is calculated as an average of the relative overlap between itself and CO_2 (12.5 W/m²/55.2 W/m²) and clouds (32.2 W/m²/ 55.2 W/m²) as well as when it is added as a third component (39.4 W/m²/ 94.9 W/m²), of course again scaled to the three components altogether to make a total of 50.0%.

With the second and third methods the reduction of the CO_2 contribution due to overlap is smaller than in the first method due to relatively low overlap to H_2O and clouds compared to the overlap between H_2O and clouds. The H_2O overlap effect in the first method is high due to the high value of the radiative forcing due to H_2O. In the two last methods the overlap effect between H_2O and clouds are distributed almost equally between the two components, therefore the cloud contribution is larger in the first method and the H_2O contribution is larger in the second and third method.

Figure 16 shows the distribution of the total radiative forcing at the tropopause when O_3, CH_4, N_2O, and halocarbons is included in addition to the three components described above when the third method is used. The total radiative forcing is now 168.6 W/m². Together O_3, CH_4, N_2O, and halocarbons only contribute about 5% to the total radiative forcing at the tropopause. In the calculation only CFC-11, CFC-12, and CCl_4 are taken into account of the halocarbons. The halocarbon contribution is small, however this contribution is from gases that only have been present in the atmosphere in the last decades, while for the other components there have been relatively small changes in the radiative forcing since pre industrial times (largest changes in the radiative forcing due to CO_2 and CH_4 since pre industrial times).

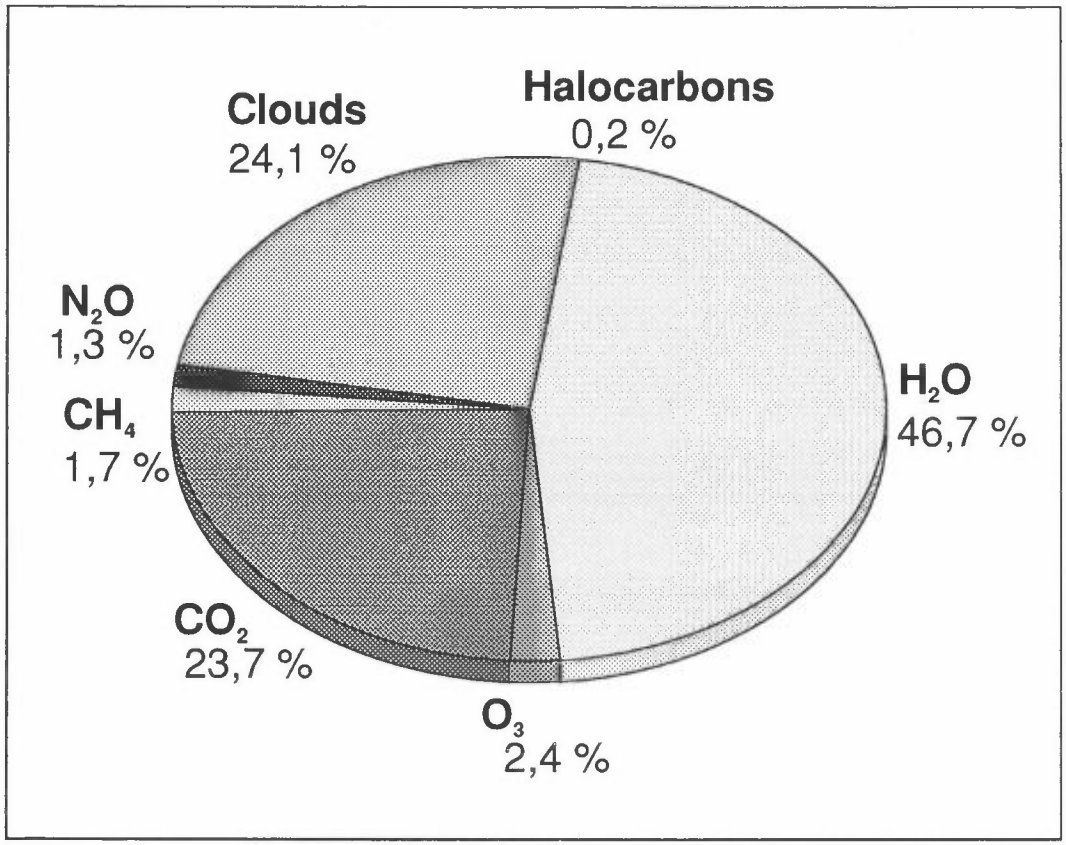

Figure 16: Distribution of the greenhouse effect at the tropopause on the infrared active gases and clouds.

Figure 17 shows distribution of the radiative forcing when clouds are not taken into account. The contribution from the various gases increase differently due to different overlap with clouds. Water vapour increases a lot and contributes almost 2/3 of the total radiative forcing. If clouds are included in addition to the greenhouse gases shown in Figure 17 the total radiative forcing increases only by 15.2%. This number is much lower than the contribution by clouds shown in Figure 16 (24.1%). In Figure 16 the overlap between gases and clouds reduces both the contribution from gases and clouds. When clouds are included in addition to the gases, the overlap between gases and clouds only reduce the clouds contribution. This shows that quite different results can be obtained by different methods. Table 7 summarizes the results performed with the OBIR model.

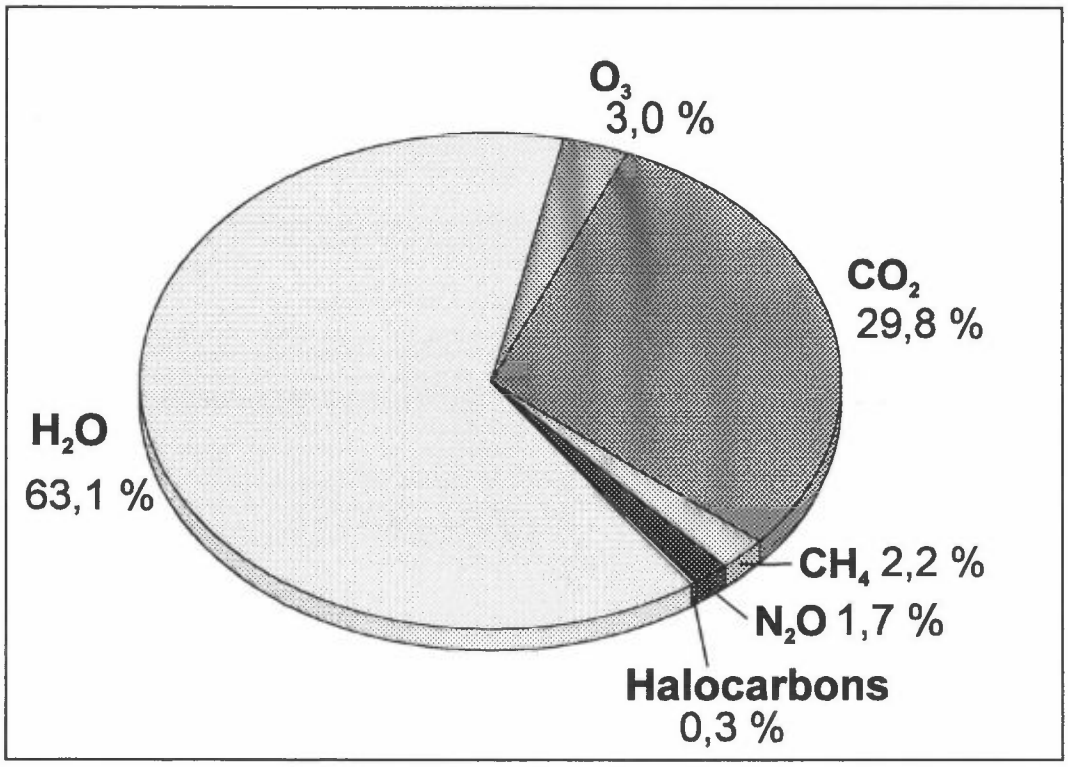

Figure 17: Same as 16, but clouds not included.

Table 7: Radiative forcing due to infrared active components in a cloudy a clear sky atmosphere.

Infrared active component	Clouds included	Clear sky
H_2O	78.7	92.4
CO_2	39.9	43.7
O_3	4.0	4.3
CH_4	2.8	3.2
N_2O	2.2	2.5
Halocarbons	0.30	0.35
Clouds	40.7	
Sum	168.6	146.4

4.4 Seasonal variations

Results up to now are only showed for yearly averages, and in many cases as global distributions. In this section we focus on the variations over the year as monthly means and global averages. First the seasonal variation of the OLR at TOA is shown in Figure 18. The OLR has the highest values in June, July, August and the lowest values in January, February, and December. The seasonal variation is more than 6 W/m2. Figure 19 shows the yearly variation of the global average radiation trapped in the atmosphere by the greenhouse gases and clouds. The same picture as in the previous figure can be recognized, with an even larger seasonal variation. The seasonal variation is about 10 W/m2. This indicates that the global

average emitted long wave radiation from surface undergo a seasonal variation of about 15 W/m2. Then the global average surface temperature must have large seasonal variation. This is due to a seasonal variation in the global average surface temperature which is 285.8 in January and 289.3 K in July.

For the CRF not only the amount of available absorbable radiation, but also the amount of clouds is important. Figure 20 shows the global average CRF at TOA as a function of month. The highest values are in May, and lowest values in March, but the variation is small; less than 1 W/m2. Figure 21 shows the global average radiative forcing due to ozone at the tropopause level. For ozone the seasonal variation follows more the same picture as for the OLR and the radiation trapped in the atmosphere than for the CRF. The highest value in June is about 10% higher than the lowest value in February.

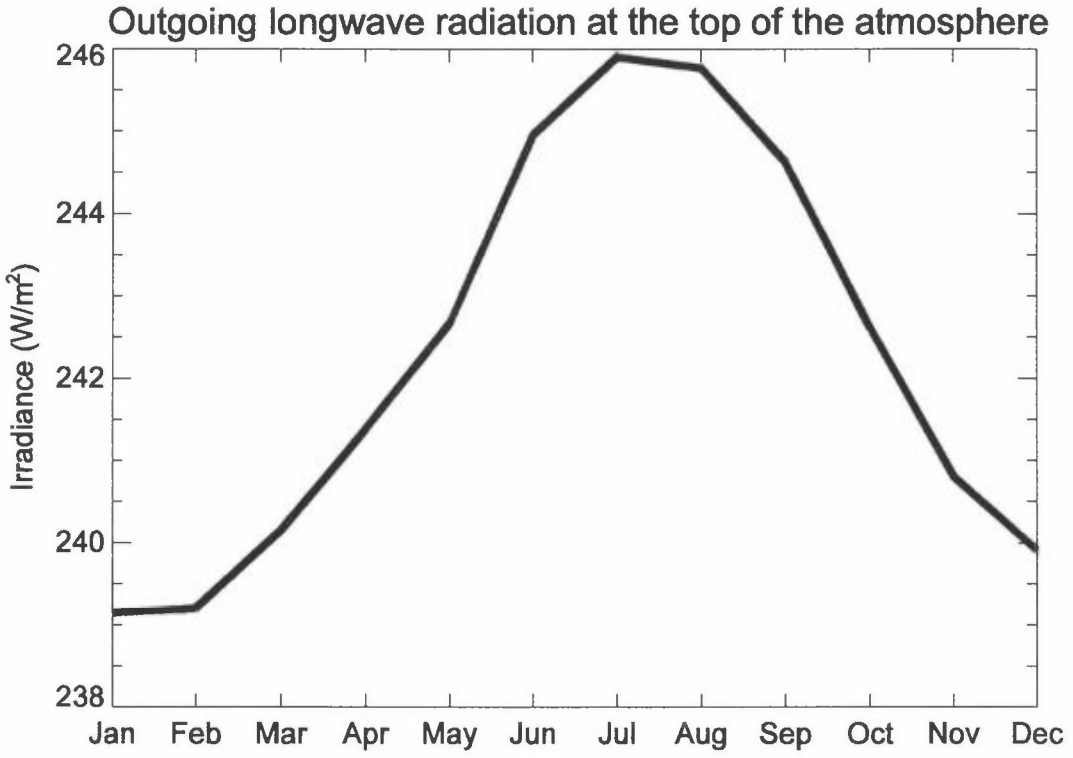

Figure 18: Seasonal variation of the global averaged outgoing long wave radiation at the top of the atmosphere given in W/m2.

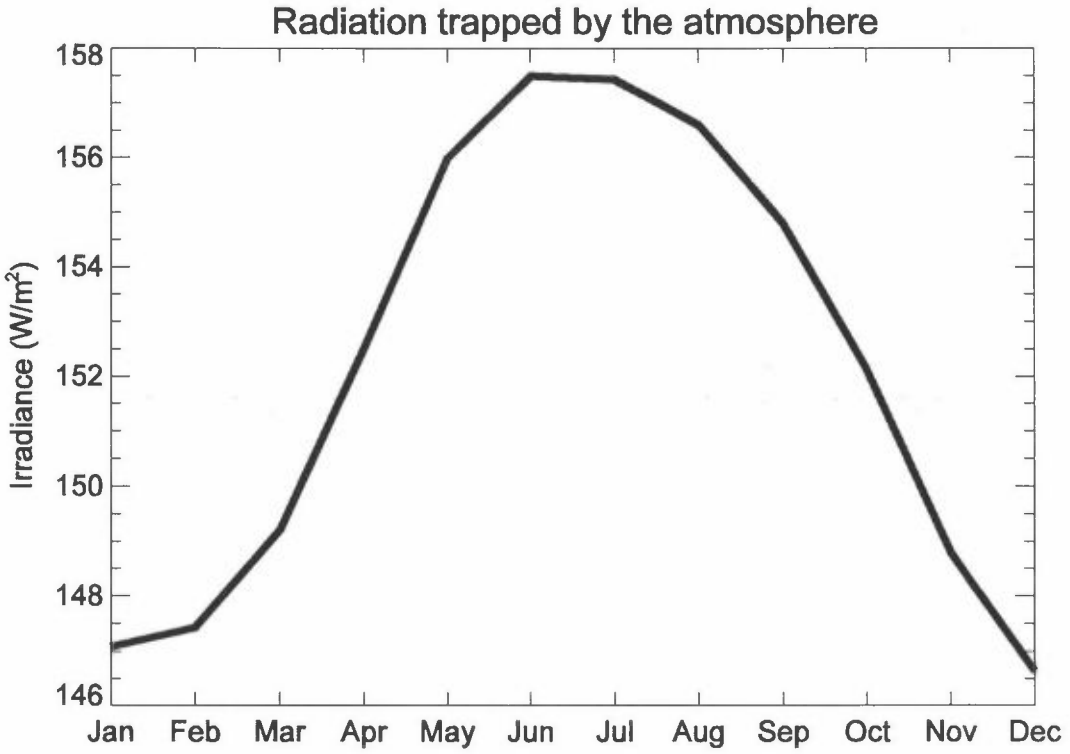

Figure 19: Seasonal variation of the global averaged trapped radiation by the atmosphere given in W/m².

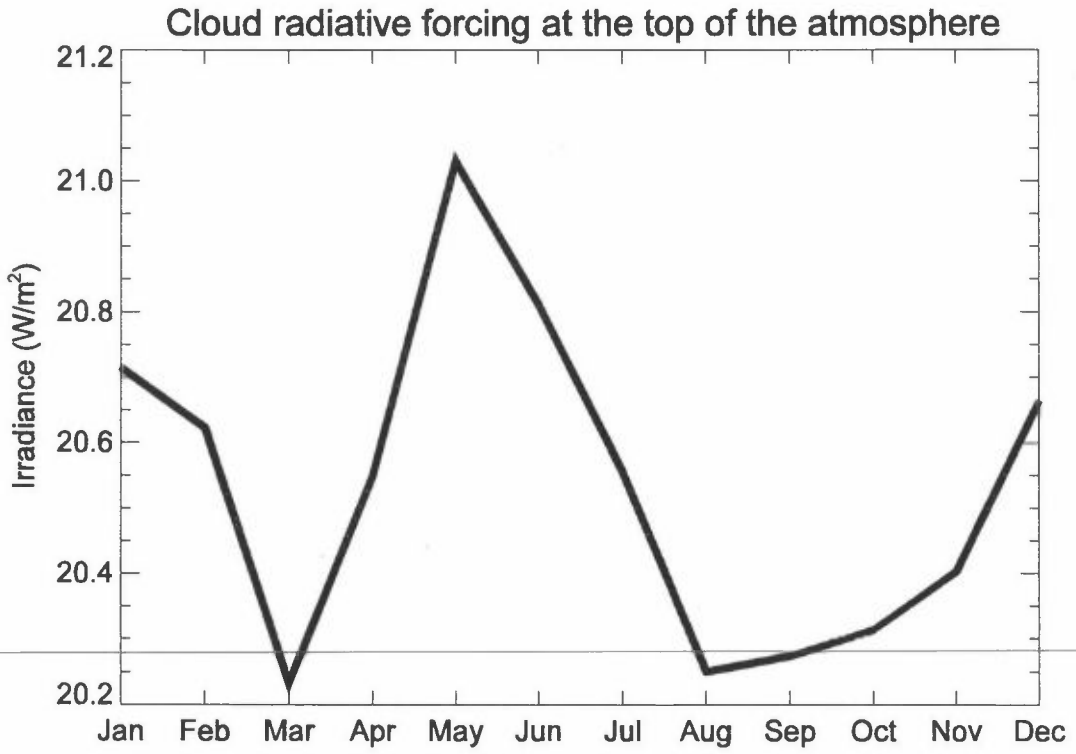

Figure 20: Seasonal variation of the global averaged cloud radiative forcing at the top of the atmosphere given in W/m².

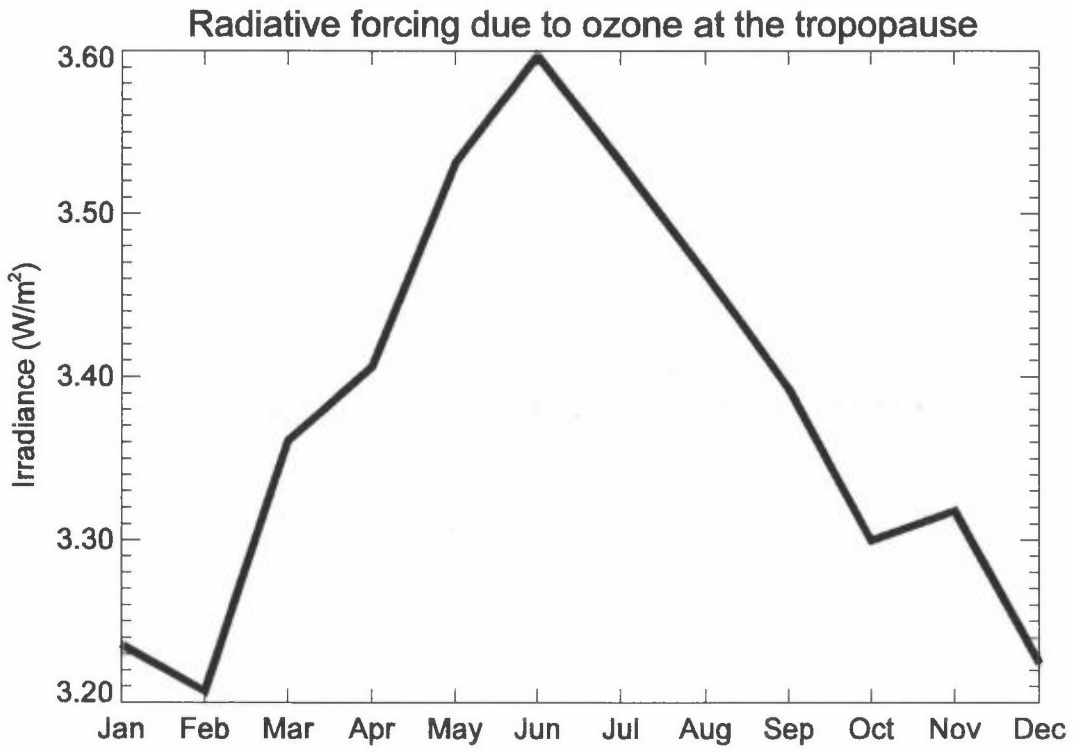

Figure 21: Seasonal variation of the global averaged radiative forcing due to ozone at the tropopause given in W/m².

5. Model comparison of radiative forcing due to ozone change

Recently a model comparison of the radiative forcing due to ozone changes has been performed (Shine et al., 1995; hereafter S95). The purpose of the study was to assess the differences in calculated radiative forcing due to differences in the radiation schemes. In the comparison an idealized atmospheric profile and ozone perturbation was used. Changes in ozone were assumed both in the troposphere and stratosphere.

In the comparison 6 groups participated, and a total of 9 different models were used. All the groups used both long wave and short wave radiation transfer schemes. The atmospheric profile used was based on the mid latitude summer (MLS) profile of McClathey et al. (1972). In addition to the MLS profile a perturbed ozone profile was used with a 10% increase of ozone in the troposphere and a decrease of 25% in the lower stratosphere. The radiative forcing was compared for instantaneous as well as adjusted radiative forcing. In the latter case the stratospheric temperature is allowed to adjust to changes in heating rates in the stratosphere.

In this study we have performed the calculations with identical input as in S95. In the short wave region the DISORT model has been used and the long wave radiative transfer calculations are performed with the OBIR model. Results from our calculations for instantaneous radiative forcing and adjusted radiative forcing are compared to the results presented in S95. Temperature changes in the

stratosphere and heating rate changes calculated by the DISORT and OBIR models are also shown.

5.1 Instantaneous radiative forcing

Figure 22 shows the short wave, long wave, and net instantaneous radiative forcing for three cases, the ALL (troposphere and stratosphere change), TROP (only change in troposphere), and STRAT (only change in stratosphere) cases. An overall good agreement between the results from the DISORT and OBIR models and the results in S95 can be observed. In the short wave calculations both the TROP and STRAT instantaneous forcing is positive, but the STRAT contribution is much larger than the TROP contribution. The ALL long wave instantaneous radiative forcing is also positive, however in this case the STRAT contribution is negative. The net radiative forcing in the ALL case is positive and is around 0.4 W/m^2.

The results from the individual models in S95 differs somewhat. It is believed that in the short wave region calculations differ due to simplifications used in the parameterizations in some models. The results in S95 for the short wave instantaneous radiative forcing in the ALL case varies is from 0.246 W/m^2 to 0.328 W/m^2, while our calculation gives 0.305 W/m^2.

In the long wave region the models in S95 can be ordered mainly into two groups. The first group consist of models including both the main 9.6 μm band of ozone and the spectroscopically weaker 14 μm band. The second group consist of models including only the 9.6 μm band of ozone. In Figure 22 only results from models representing both bands are presented. The long wave instantaneous radiative forcing calculated by the OBIR model is 0.081 W/m^2, which is in accordance with the average in S95, where the results varied from 0.072 W/m^2 to 0.096 W/m^2.

Figure 23 shows results when only the 9.6 μm band of ozone is included. For the TROP and the STRAT cases the sign is the same as when the 14 μm band was included. The absolute values are lower, but the change is larger in the STRAT case than in the TROP case. This indicates that the 14 μm band of ozone is more important in the stratosphere than in the troposphere. Two of the groups in S95 have performed calculations both with and without the 14 μm band of ozone. When the 14 μm band of ozone was neglected, results showed that the radiative forcing for the ALL case increased with 0.018 W/m^2 and 0.031 W/m^2, while the results from the OBIR calculation show an increase of the radiative forcing corresponding to 0.015 W/m^2.

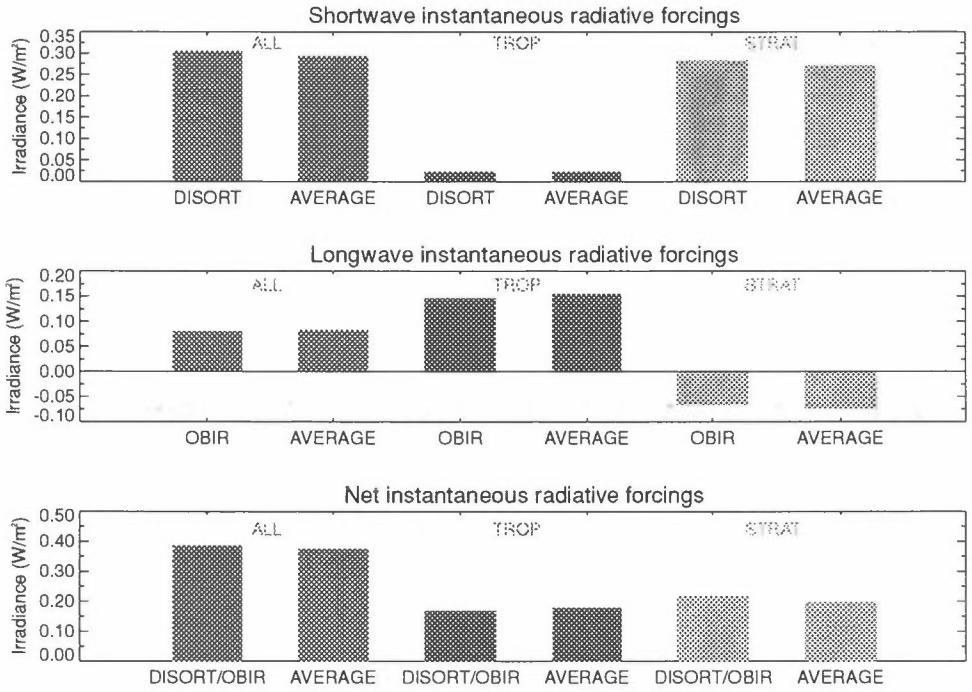

Figure 22: Shortwave, longwave, and net instantaneous radiative forcings due to change in tropospheric ozone (TROP), stratospheric ozone (STRAT) and the combined effect (ALL) as the ozone changes in S95. Results are for the DISORT and OBIR models and the averages of the models in S95. The results from the longwave models are from calculations performed with both the 14 og 9.6 μm band of ozone.

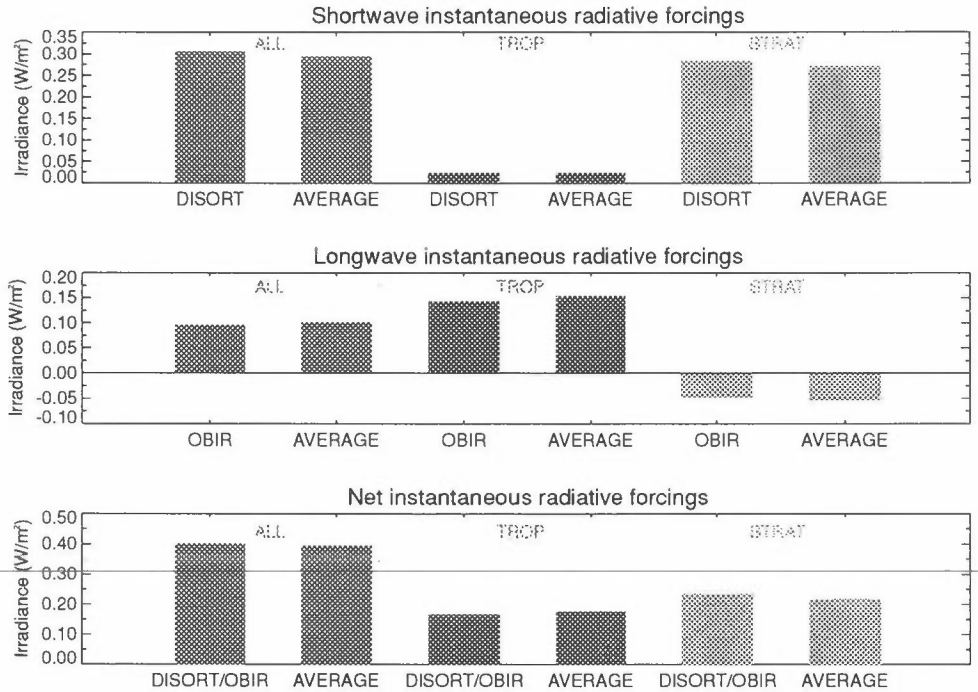

Figure 23: As for Figure 22, but only the 9.6 μm band are included in the long-wave calculations.

5.2 Adjusted radiative forcing

In the adjusted radiative forcing calculations the stratospheric temperature has been allowed to adjust to the changes in heating rates in the stratosphere. This has been done under the assumption that the changes in temperatures are controlled by the changes in convergence in radiative fluxes alone, i.e. the so-called fixed dynamical heating approximation. Figure 24 shows the vertical profile of the temperature change in the stratosphere as calculated by the DISORT and OBIR models. Figure 25 and Figure 26 show the change in short wave heating rates and long wave heating rates respectively. The region where the largest temperature change is estimated, the lower stratosphere, is about the same in our calculations as in S95. The calculated temperature change in our model is about -2.7 K whereas the calculated temperature change in S95 was -2.0 to -2.5 K. This difference is mainly due to larger heating rate change in the long wave OBIR calculations than in the S95 models in this region. The short wave heating rates change calculated here compares well to the results of the other models in S95, this is also the case for the long wave heating rate change and temperature change for other regions than the lower stratosphere.

Figure 27 shows the short wave, long wave, and net adjusted radiative forcing for the ALL, TROP, and STRAT cases for calculations by the DISORT and OBIR models, as well as the average results in S95. Results from the short wave calculations show little differences compared to the instantaneous radiative forcing calculations. On the other hand, results from the long wave calculations show a considerable difference compared to the instantaneous radiative forcing calculations. Even the sign changes for the ALL case and is negative in the net adjusted case. The largest change is in the STRAT case, while in the TROP case the change is relatively small. The average of the adjusted long wave radiative forcing in S95 in the ALL case is somewhat lower in absolute value than the result of the OBIR model (-0.310 W/m^2 compared to -0.328 W/m^2). A relatively small variation among the results in S95, from -0.288 W/m^2 to -0.335 W/m^2, can be noticed for this case. In our calculations the long wave contribution dominates over the short wave contribution, resulting in a net adjusted radiative forcing that is negative. This is also the case in all the models in S95 that include both ozone bands.

Figure 28 shows similar results as in Figure 27, but with the difference that only the 9.6 μm band of ozone is taken into account. The absolute importance of the 14 μm band is larger for the adjusted radiative forcing than for the instantaneous radiative forcing, but the relative importance is smaller. The 14 μm band of ozone is important for the sign of the net radiative forcing. In our calculations the net adjusted radiative forcing is zero when the 14 μm band is omitted. In most of the other models in S95 inclusion of the 14 μm band leads to a change in the net adjusted radiative forcing from negative to positive values.

Table 8 summarizes the results from the DISORT and OBIR model for the instantaneous and adjusted radiative forcing. In the infrared region results are presented in the case when both ozone bands have been included (OBIR 1) as well as the case when only the 9.6 μm band was taken into account (OBIR 2).

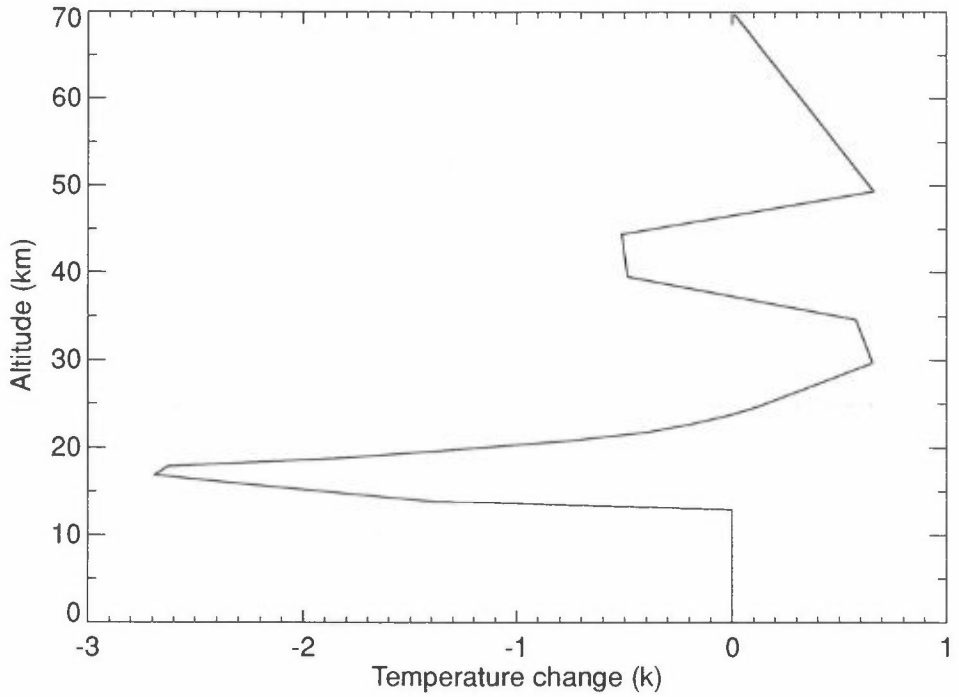

Figure 24: Vertical profile of the change in the temperature where the stratospheric temperature has been allowed to adjust to the changes in heating rates in the stratosphere using the fixed dynamical heating approximation due to changes in ozone as in S95 as calculated with DISORT and OBIR models.

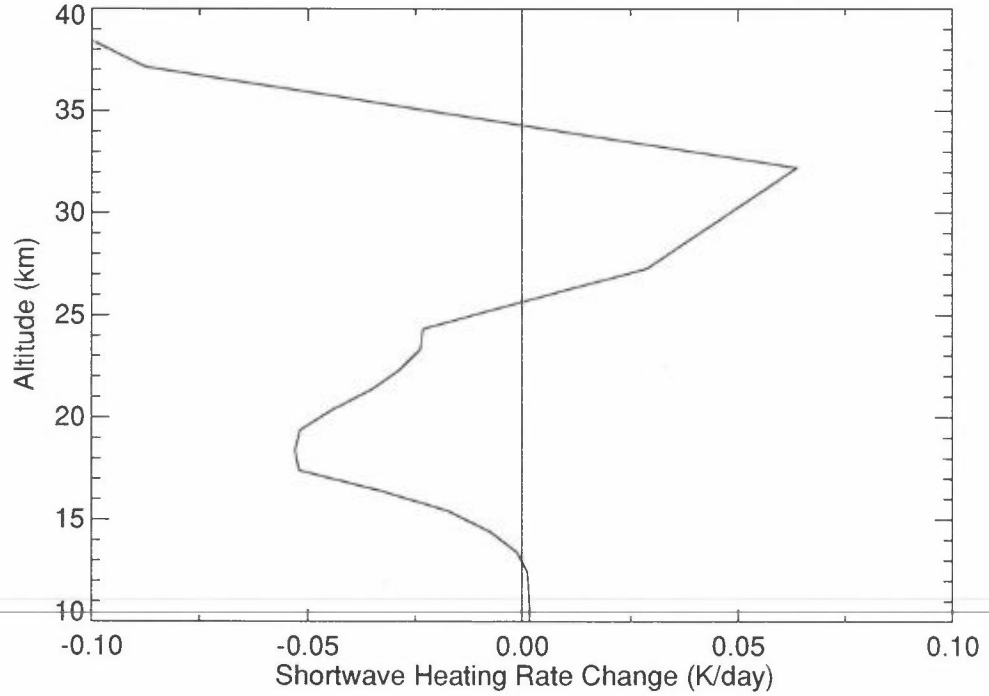

Figure 25: Shortwave heating rate change due to change in ozone as calculated with the DISORT model in K/day.

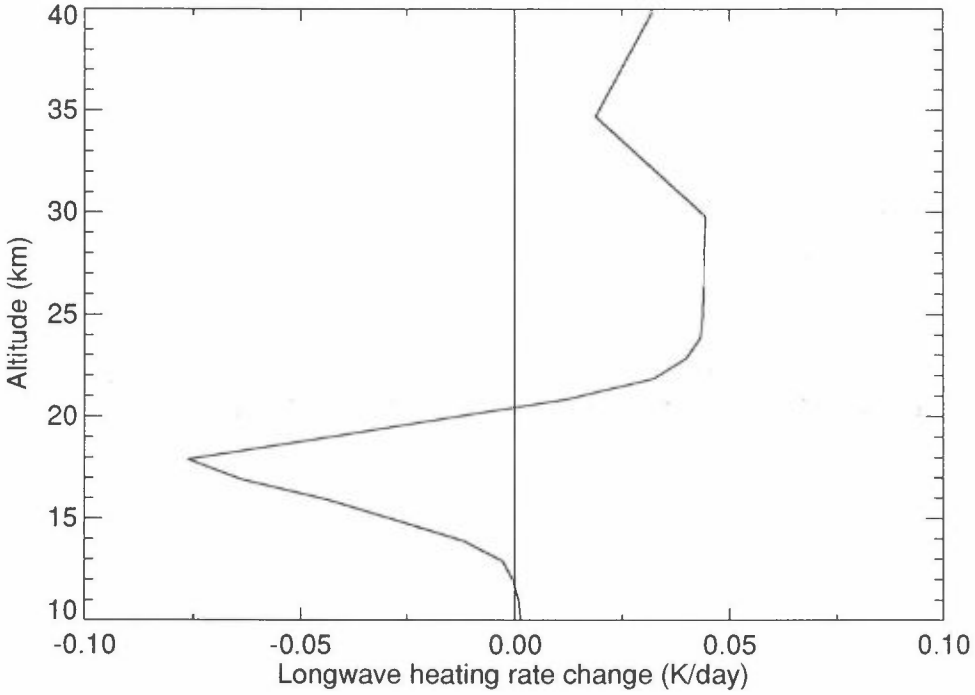

Figure 26: As for the Figure 26, but for longwave heating rate change and calculated with the OBIR model.

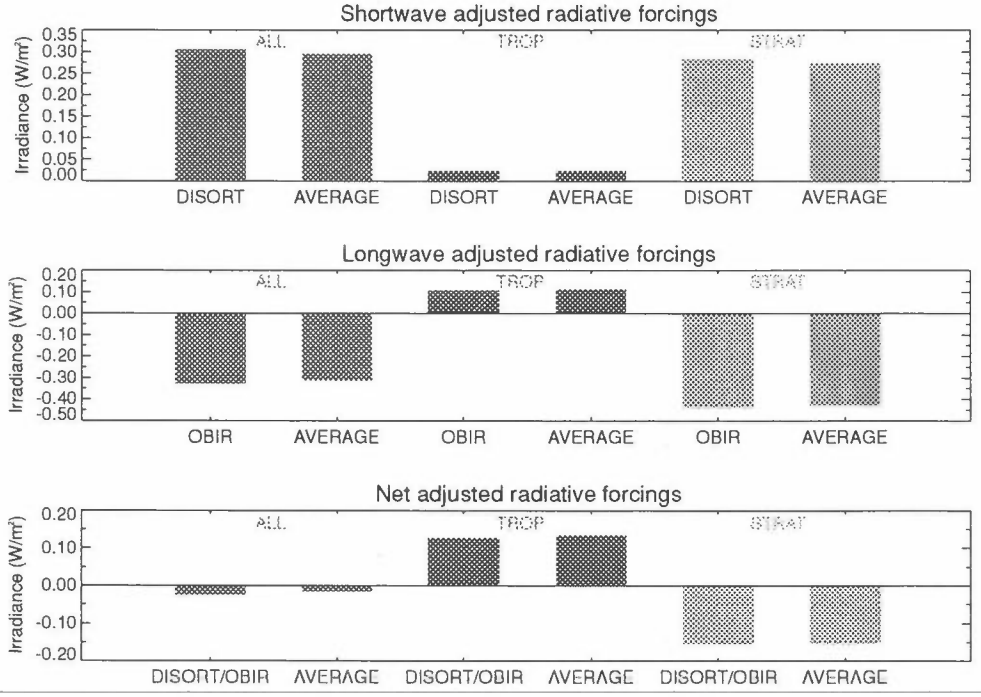

Figure 27: As for Figure 22, but for adjusted radiative forcings.

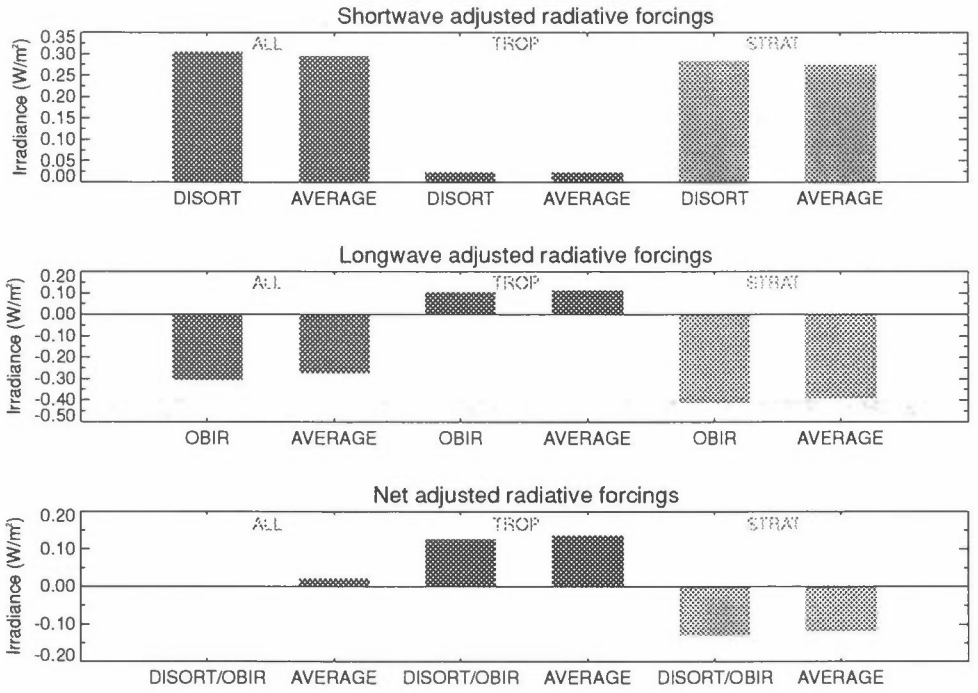

Figure 28: As for Figure 22, but for adjusted radiative forcing and only the 9.6 μm band are included in the longwave calculations.

Table 8: Instantaneous and adjusted radiative forcing due to change in ozone as defined in S95. Calculations are performed with the DISORT and OBIR models. Results in the long wave range are presented for cases when the 14 μm band of ozone has been included (OBIR-1) and neglected (OBIR-2), respectively. Changes in tropospheric ozone (TROP), stratospheric ozone (STRAT) and the combined effect (ALL) have been estimated based on the ozone changes used in S95.

Instantaneous radiative forcing:

	ALL			TROP			STRAT		
	SW	**LW**	**NET**	**SW**	**LW**	**NET**	**SW**	**LW**	**NET**
DISORT/OBIR (1)	0.305	0.081	0.386	0.023	0.146	0.169	0.282	-0.065	0.217
DISORT/OBIR (2)	0.305	0.096	0.401	0.023	0.143	0.166	0.282	-0.047	0.235

Adjusted radiative forcing:

	ALL			TROP			STRAT		
	SW	**LW**	**NET**	**SW**	**LW**	**NET**	**SW**	**LW**	**NET**
DISORT/OBIR (1)	0.305	-0.328	-0.023	0.023	0.105	0.128	0.282	-0.435	-0.153
DISORT/OBIR (2)	0.305	-0.305	0.000	0.023	0.103	0.126	0.282	-0.410	-0.128

6. Acknowledgements

This work has been sponsored by the Nordic Environmental Research Program under the project "Ozone a climate gas", by the Climate and ozone program of the Norwegian Research Council, as well as by contract EV5V-CT94-0492 of the European Commission.

7. References

Ardanuy, P.E., Stowe, L.L., Gruber, A. and Weiss, M. (1991) Shortwave, longwave and net cloud-radiative forcing as determined from Nimbus 7 observations. *J. Geophys. Res., 96,* 18537–18549.

Dahlback, A. and Stamnes, K. (1991) A new spherial model for computing the radiation field available for photolysis and heating at twilight. *Planet. Space Sci., 39,* 671–683.

Dahlback, A., Rairoux, P., Stein, B., Del Gausta, M., Kyrö, E., Stefanutti, L., Larsen, N. and Braathen, G. (1994) Effects of stratospheric aerosols from the Mt. Pinatubo eruption on ozone measurements at Sodankylä, Finland in 1991/1992. *Geophys. Res. Lett., 13,* 1399–1402.

Harrison, E.F., Minnis, P., Barkstrom, B.R., Ramanathan, V., Cess, R.D. and Gibson, G.G. (1990) Seasonal variation of cloud radiative forcing derived from the Earth Radiation Budget Experiment. *J. Geophys. Res., 95,* 18687–18703.

Hartman, D.L., Ockert-Bell, M.E. and Michelsen, M.L. (1992) The effect of cloud type on earth's energy balance: Global analysis. *J. Clim., 5,* 1281–1304.

IPCC (1994) Radiative forcing of climate change. Intergovernmental Panel on Climate Change. New York, Cambridge Univ. Press.

Liang, X.-Z. and Wang, W.-C. (1995) A GCM study of the climatic effect of 1979-1992 ozone trend, In: *Atmospheric ozone as a climate gas*. Ed. by W.-C. Wang and I.S.A. Isaksen. Berlin, Springer (NATO ASI. Series I. Global Environmental Change, 32).

McClatchey, R.A., Fenn, R.W., Selby, J.E.A., Volz, F.E. and Garing, J.S. (1972) Optical properties of the atmosphere. Bedford Mass., Air Force Cambridge Res. Lab., Hanscom Air Force Base (Rep. AFCRL-72-0497).

Myhre G., and Stordal, F. (1995) An updated version of the Oslo Broad band InfraRed (OBIR) model. Institute for Geophysics, University of Oslo (Report No. 93).

Ramanathan, V. and Dickinson, R.E. (1979) The role of stratospheric ozone in the zonal and seasonal radiative energy balance of the earth-troposphere system. *J. Atmos. Sci., 36,* 1084–1104.

Ramanathan, V., Cess, R.D., Harrison, E.F., Minnis, P., Barkstrom, B.R., Ahmad, E. and Hartmann, D. (1989) Cloud -radiative forcing and climate: Results from the Earth Radiation Budget Experiment. *Science, 243,* 57–63.

Rossow, W.B. and Schiffer, R.A. (1991) ISCCP cloud data products. *Am. Meteorol. Soc. Bull., 72,* 2–20.

Rossow, W.B. and Zhang, Y.-C. (1995) Calculation of surface and top of atmosphere radiative fluxes from physical quantities based on ISCCP data sets 2. Validation and first results. *J. Geophys. Res., 100,* 1167–1197.

Shine, K.P., Briegleb, B.P., Grossman, A.S., Hauglustaine, D., Mao, H., Ramaswamy, V., Schwarzkopf, M.D., Van Dorland, R. and Wang, W.-C. (1995) Radiative forcing due to changes in ozone – A comparison of different codes. In: *Atmospheric ozone as a climate gas*. Ed. by W.-C. Wang and I.S.A. Isaksen. Berlin, Springer (NATO ASI. Series I. Global Environmental Change, 32).

Stordal, F. (1988) A wide band model for transfer of infrared radiation: Altidue latitudinal and yearly variation of cooling rates in the troposphere and the stratosphere. University of Oslo, Institute for Geophysics (Report no. 68).

Norwegian Institute for Air Research (NILU)
P.O. Box 100, N-2007 Kjeller – Norway

REPORT SERIES SCIENTIFIC REPORTS	REPORT NO. OR 26/96	ISBN-82-425-0768-6	
DATE 16/7-96	SIGN. P.R.	NO. OF PAGES 39	PRICE NOK 60.-

TITLE	PROJECT LEADER
Radiative impacts of ozone and other radiatively active components	F. Stordal
	NILU PROJECT NO. O-93003/O-96044
AUTHOR(S) Frode Stordal, Terje A. Larsen, Gunnar Myhre og Lars Zetterberg	CLASSIFICATION * A
	CONTRACT REF.

REPORT PREPARED FOR:

Nordic Council of Ministers (NMR)
Store Strandstræde 18
DK-1255 COPENHAGEN K
DENMARK

The Research Council of Norway (NFR)
P.O. Box 2700 St. Hanshaugen
N-0131 OSLO
NORWAY

ABSTRACT
Radiative transfer calculations have been performed with two models of infrared radiation (broad band and line-by-line) and one model for ultraviolet and visible radiation (discrete ordinate method). The calculations are aimed at quantifying the radiative effects of radiatively active gases, in particular ozone. Seasonal variations and trends in the the radiative forcing due to presence of ozone in the atmosphere is studied, based on observed ozone profiles from ozone soundings at selected Nordic locations.

NORWEGIAN TITLE
Virkninger av ozon og andre strålingsaktive gasser på atmosfærens strålingsbudsjett

KEYWORDS		
Radiative forcing	Climate change	Ozone

ABSTRACT (in Norwegian)

* *Classification*
- *A Unclassified (can be ordered from NILU)*
- *B Restricted distribution*
- *C Classified (not to be distributed)*